PHYSIOLOGY

Evidence for a neuromuscular circuit involving hypothalamic interleukin-6 in the control of skeletal muscle metabolism

**Carlos Kiyoshi Katashima[1]†, Thayana de Oliveira Micheletti[2]†, Renata Rosseto Braga[1], Rodrigo Stellzer Gaspar[1,3], Ludger J. E. Goeminne[4], Alexandre Moura-Assis[3], Barbara Moreira Crisol[1], Rafael S. Brícola[1], Vagner Ramon R. Silva[1], Camila de Oliveira Ramos[5], Alisson L. da Rocha[6,7], Mariana Rosolen Tavares[8], Fernando Moreira Simabuco[8], Valquiria Aparecida Matheus[9], Lucas Buscaratti[10], Henrique Marques-Souza[10], Patricia Pazos[11], David Gonzalez-Touceda[11], Sulay Tovar[11], María del Carmen García[11], Jose Cesar Rosa Neto[12], Rui Curi[13,14], Sandro Massao Hirabara[14], Patrícia Chakur Brum[15], Patrícia Oliveira Prada[2], Leandro P. de Moura[1,16], José Rodrigo Pauli[1,16], Adelino S. R. da Silva[6,7], Dennys Esper Cintra[5], Licio A. Velloso[2,3], Eduardo Rochete Ropelle[1,2,3,16]*

Hypothalamic interleukin-6 (IL6) exerts a broad metabolic control. Here, we demonstrated that IL6 activates the ERK1/2 pathway in the ventromedial hypothalamus (VMH), stimulating AMPK/ACC signaling and fatty acid oxidation in mouse skeletal muscle. Bioinformatics analysis revealed that the hypothalamic IL6/ERK1/2 axis is closely associated with fatty acid oxidation– and mitochondrial-related genes in the skeletal muscle of isogenic BXD mouse strains and humans. We showed that the hypothalamic IL6/ERK1/2 pathway requires the α2-adrenergic pathway to modify fatty acid skeletal muscle metabolism. To address the physiological relevance of these findings, we demonstrated that this neuromuscular circuit is required to underpin AMPK/ACC signaling activation and fatty acid oxidation after exercise. Last, the selective down-regulation of IL6 receptor in VMH abolished the effects of exercise to sustain AMPK and ACC phosphorylation and fatty acid oxidation in the muscle after exercise. Together, these data demonstrated that the IL6/ERK axis in VMH controls fatty acid metabolism in the skeletal muscle.

INTRODUCTION

The hypothalamus regulates metabolic processes (*1*, *2*) and functions of peripheral organs and glands such as the liver (*3*), white adipose tissue (*4*), brown adipose tissue (*5*), thyroid gland (*6*), and others. Neuronal activity in the ventromedial hypothalamus (VMH) controls energy expenditure and skeletal muscle metabolism, including fatty acid oxidation and glucose metabolism (*7*, *8*). In this context, hormones and neuropeptides, such as leptin and orexin, can modify muscle metabolism in murine models by stimulating VMH neurons (*7*, *9*).

The central action of interleukin-6 (IL6) exerts distinct functions in the metabolism of mammals (*10*–*12*). Hypothalamic IL6 has been implicated in controlling energy expenditure (*13*) and food consumption (*10*, *11*). The metabolic improvements induced by physical exercise require the hypothalamic IL6 action in obese rodents (*14*). Here, we hypothesized that hypothalamic IL6 might control skeletal muscle metabolism. Thus, we sought to determine the existence of a neuromuscular circuit involving hypothalamic IL6 action in the VMH nucleus toward skeletal muscle metabolism.

RESULTS

Hypothalamic IL6 stimulates fatty acid metabolism in skeletal muscle

An interaction graph using the Genotype-Tissue Expression (GTEx) human database (*15*) from 81 individuals revealed a positive association (red lines) between hypothalamic *IL6* gene expression and lipid metabolism– and mitochondrial-related genes in the skeletal muscle (Fig. 1A). No correlation was observed between the hypothalamic *IL6* gene and glucose metabolism– and protein synthesis–related genes (Fig. 1A). Hypothalamic *IL6* gene expression showed a positive correlation (red lines) with lipid metabolism–related

[1]Laboratory of Molecular Biology of Exercise (LaBMEx), School of Applied Sciences, University of Campinas (UNICAMP), Limeria, São Paulo 13484-350, Brazil. [2]Faculty of Medical Sciences, Department of Internal Medicine, University of Campinas (UNICAMP), Limeira, São Paulo, Brazil. [3]Laboratory of Cell Signaling, Obesity and Comorbidities Research Center, University of Campinas (UNICAMP), Limeira, São Paulo, Brazil. [4]Laboratory of Integrative Systems Physiology, Interfaculty Institute of Bioengineering, École Polytechnique Fédérale de Lausanne, Lausanne, Switzerland. [5]Laboratory of Nutritional Genomic, School of Applied Sciences, University of Campinas (UNICAMP), Limeira, São Paulo 13484-350, Brazil. [6]Postgraduate Program in Rehabilitation and Functional Performance, Ribeirão Preto Medical School, University of São Paulo (USP), Ribeirão Pretol, São Paulo, Brazil. [7]School of Physical Education and Sport of Ribeirão Preto, University of São Paulo, Ribeirão Preto, São Paulo, Brazil. [8]Multidisciplinary Laboratory of Food and Health (LabMAS), School of Applied Sciences (FCA), University of Campinas (UNICAMP), Limeira, São Paulo, Brazil. [9]Department of Genetics, Evolution, Microbiology and Immunology, Institute of Biology, University of Campinas (UNICAMP), Limeira, São Paulo, Brazil. [10]Department of Biochemistry and Tissue Biology, Institute of Biology, University of Campinas (UNICAMP), Limeira, São Paulo, Brazil. [11]Department of Physiology, Research Center of Molecular Medicine and Chronic Diseases (CIMUS) and CIBER Fisiopatología Obesidad y Nutrición (CB 06/03), Instituto de Salud Carlos III (ISCIII, Ministerio de Economía y Competitividad (MINECO), University of Santiago de Compostela, Santiago de Compostela 15782, Spain. [12]Immunometabolism Research Group, Institute of Biomedical Sciences, University of São Paulo (USP), São Paulo 05508-900, Brazil. [13]Department of Physiology and Biophysics, Institute of Biomedical Sciences, University of São Paulo (USP), São Paulo 05508-900, Brazil. [14]Institute of Physical Activity Sciences and Sports, Cruzeiro do Sul University, São Paulo 01506-000, Brazil. [15]School of Physical Education and Sport, University of São Paulo (USP), São Paulo 05508-030, Brazil. [16]CEPECE—Center of Research in Sport Sciences, School of Applied Sciences, University of Campinas (UNICAMP), Limeira, São Paulo 13484-350, Brazil.
*Corresponding author. Email: eduardoropelle@gmail.com
†These authors contributed equally to this work.

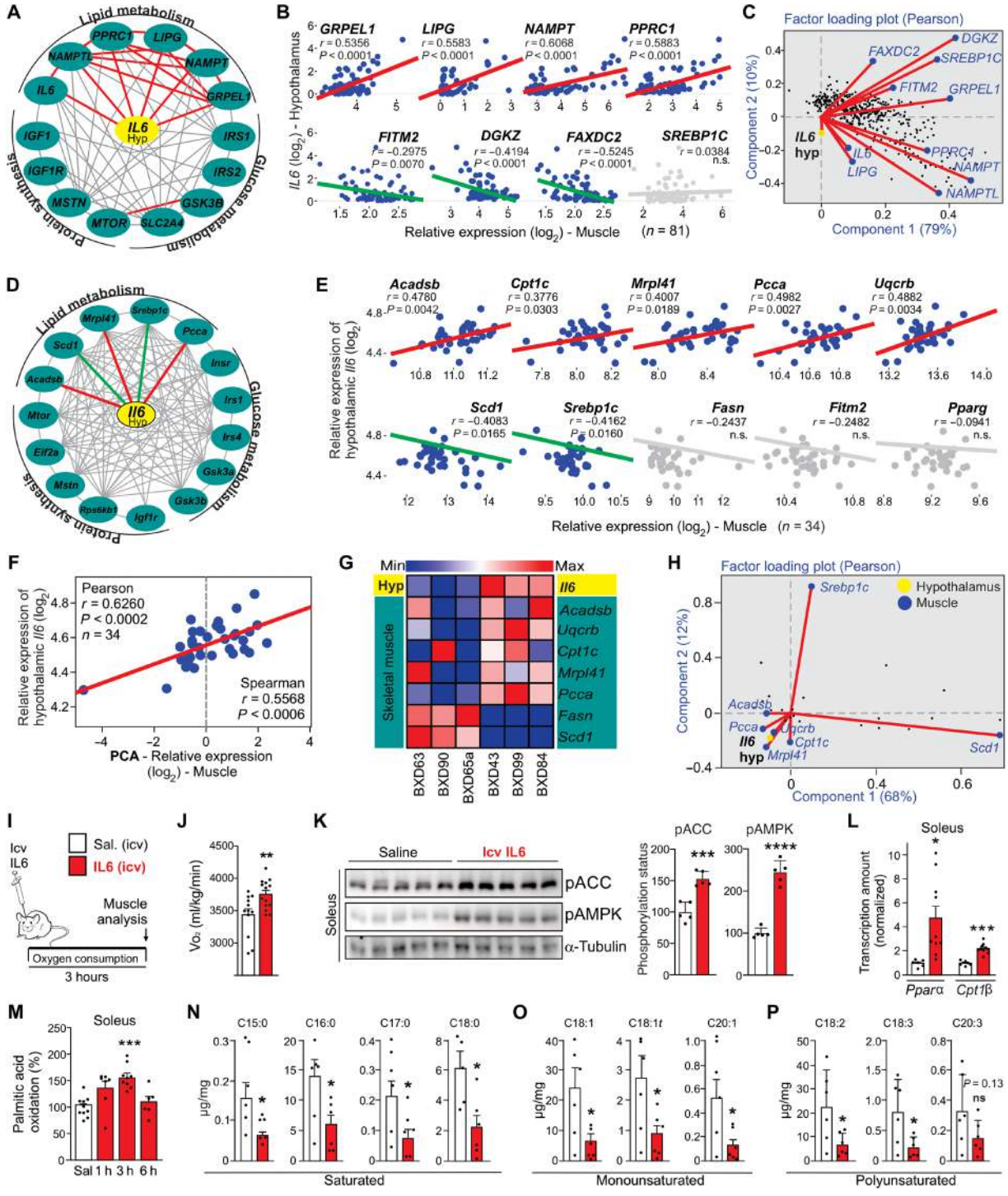

Fig. 1. Hypothalamic IL6 induces fatty acid oxidation in muscle. (**A**) Interaction and (**B**) Pearson's correlation graphs show the correlation between hypothalamic *IL6* gene expression and several genes of human skeletal muscle. Gray line represents no correlation. Pearson's correlation $r \geq |0.5|$ and $P < 0.05$ ($n = 81$). n.s., not significant. (**C**) Factor loading plot: angles more than 90° between gene vectors represent a negative correlation. (**D**) Interaction and (**E**) Pearson's correlation graphs. Pearson's correlation $r \geq |0.35|$ and $P < 0.05$ ($n = 34$). (**F**) PCA value was obtained using *Acadsb*, *Cpt1c*, *Mrpl41*, *Pcca*, and *Uqcrc* relative expression in the muscle of BXD mice. (**G**) Heatmap graph using hypothalamic and muscle transcripts from six different BXD mouse strains. (**H**) Factor loading plot (biplot) by using BXD cohort. (**I**) Experimental design using male C57BL6/J mice. (**J**) Oxygen consumption during 3 hours after recombinant IL6 intracerebroventricular (icv) microinjection (200 ng) ($n = 11$ to 14). (**K**) ACC and AMPK phosphorylation in the soleus muscle mice ($n = 5$). (**L**) *Cpt1*β and *Pparα* mRNA in the soleus muscle 3 hours after recombinant IL6 intracerebroventricular microinjection ($n = 6$ to 10). (**M**) Palmitic acid oxidation assay in the soleus muscle in mice intracerebroventricularly injected with IL6 ($n = 6$ to 10). (**N** to **P**) Determination of fatty acid fractions in the gastrocnemius muscle 3 hours after recombinant IL6 intracerebroventricular microinjection. Unpaired *t* test was used in (J) to (L) and (N) to (P). One-way analysis of variance (ANOVA) was used for statistical analysis in (M). *$P < 0.05$, **$P < 0.01$, ***$P < 0.001$, and ****$P < 0.0001$ versus saline.

genes (Fig. 1B, top panels) and a negative correlation (green lines) with lipid biosynthesis–related genes (Fig. 1B, bottom panels). These data were confirmed by a two-factor analysis (Fig. 1C).

We next used analyses using system data from a mouse genetic reference population derived from crosses of C57BL/6J and DBA/2J inbred strains, named BXD (*16*), geared toward multiscalar integration of traits. This dataset also showed positive interaction between hypothalamic *Il6* gene expression and gene sets involved in fatty acid oxidation in the skeletal muscle (red lines). Conversely, negative interaction (green lines) was observed between hypothalamic *Il6* gene expression and expression of some markers of lipid biosynthesis in the skeletal muscle of BXD mice (Fig. 1, D and E). There was no interaction between hypothalamic *Il6* gene expression and glucose metabolism– or protein synthesis–related genes (Fig. 1D). Principal components analysis (PCA) confirmed a strong positive correlation between hypothalamic *Il6* levels and lipid oxidation– and mitochondrial-related genes in the muscle (Fig. 1F). The heatmap graph revealed that specific strains of BXD mice with low levels of hypothalamic *Il6* gene expression (BXD63, BXD90, and BXD65a) displayed high levels of transcripts related to skeletal muscle lipid biosynthesis (Fig. 1G). Conversely, BXD families with high levels of hypothalamic *Il6* gene expression (BXD43, BXD99, and BXD84) present high lipid oxidation– and mitochondrial-related genes in the skeletal muscle (Fig. 1G). The two-factor loading plots confirmed that the hypothalamic *Il6* gene expression is positively correlated with fatty acid oxidation markers (*Acadsb*, *Cpt1c*, *Mrpl41*, *Pcca*, and *Uqcrc*) and showed a negative correlation with markers of lipid biosynthesis (*Srebp1c* and *Scd1*) in the skeletal muscle of strains of genetically diverse BXD mice (Fig. 1H).

Beyond the genetic variation and correlative analyses, we tested our hypothesis experimentally by using intracerebroventricular mouse recombinant IL6 microinjection in C57BL6/J mice (Fig. 1I). Recombinant IL6 (200 ng) increased oxygen consumption (Fig. 1J) and stimulated critical markers involved in fatty acid oxidation in the soleus muscle, including acetyl–coenzyme A carboxylase 1 (ACC^{Ser79}) and AMP-activated protein kinase ($AMPK^{Thr172}$) phosphorylation (Fig. 1K) and carnitine palmitoyltransferase I (*Cpt1*β) and peroxisome proliferator–activated receptor α (*Ppar*α) gene expression (Fig. 1L). Recombinant IL6 intracerebroventricular infusion induced transient fatty acid oxidation in the soleus muscle, peaking 3 hours after the central injection (Fig. 1M). To assess the impact of hypothalamic IL6 on skeletal muscle lipid metabolism, mass spectrometry analysis was performed using the same experimental design. The central action of IL6 markedly reduced the amount of fraction of saturated (C15:0, C16:0, C17:0, and C18:0), monounsaturated (C18:1, C18:1*t*, and C20:1), and polyunsaturated (18:2, 18:3, and 20:3) fractions of fatty acids in the skeletal muscle (Fig. 1, N to P, and fig. S1A). Similar to the soleus muscle, high levels of AMPK phosphorylation were detected in the gastrocnemius muscle (fig. S1B). This effect was more discrete in the adipose tissue once IL6 central injection increased AMPK phosphorylation in epididymal, but not subcutaneous, adipose tissue (fig. S1, C and D).

It has been described that residual endotoxin contaminations in commercial recombinant proteins are sufficient to elicit biological effects in recipient cells (*17*). To confirm that central IL6, but not the residual lipopolysaccharide (LPS), stimulates AMPK/ACC phosphorylation in the skeletal muscle, mouse recombinant IL6 was intracerebroventricularly injected in wild-type and endotoxin nonsensitivity mice (TLR4KO) (*18*, *19*). This experiment demonstrated that IL6 intracerebroventricular injection increased AMPK phosphorylation in the soleus muscle of both wild-type and TLR4KO mice (fig. S1E), confirming the specificity of IL6 biological effect in this neuromuscular circuit.

Central IL6 enhances the muscle lipid metabolism through hypothalamic ERK stimulation

Previous studies have shown a functional connection between VMH and muscle metabolism (*7*, *8*). In addition, extracellular signal–regulated kinase 1/2 (ERK1/2) in VMH elicits signals from the central nervous system toward the skeletal muscle (*20*). Curiously, IL6 can induce ERK1/2 phosphorylation in neuronal cells (*21*, *22*). Thus, we monitored IL6/ERK signaling in our model. We found the presence of IL6 receptor (IL6R) in different hypothalamic nuclei, particularly in the arcuate and ventromedial nuclei (fig. S1, F and G). Next, recombinant IL6 was injected directly into VMH of mice on one side, and a vehicle was injected into the contralateral VMH of the same animal. This experimental approach demonstrated IL6 injection–induced $ERK1/2^{Thr202/Tyr204}$ phosphorylation in VMH of mice (Fig. 2A). This finding was confirmed by Western blotting analysis in hypothalamus and isolated VMH samples from IL6 intracerebroventricularly injected mice (Fig. 2, C and D).

Confocal microscopy revealed positive cells for ERK1/2 phosphorylation in IL6Rα-expressing neurons in the VMH of mice (fig. S2A). We found several phospho-ERK (pERK)–positive stainings in neurons of VMH after recombinant IL6 injection (Fig. 2B). In addition, recombinant IL6 stimulated ERK1/2 phosphorylation in Neuro2A (N2A) cells (Fig. 2E). Together, our data showed the potential of IL6 in stimulating ERK1/2 phosphorylation in neuronal cells.

To test whether the hypothalamic IL6/ERK1/2 axis is involved in skeletal muscle lipid metabolism, PD98059, a mitogen-activated protein kinase (MAPK) kinase (MEK)/ERK signaling pharmacological inhibitor, or saline was intracerebroventricularly administered 30 min before the intracerebroventricular microinjection of recombinant IL6, as detailed in the experimental design (Fig. 2F). Notably, PD98059 abolished hypothalamic IL6-induced ACC and AMPK phosphorylation (Fig. 2G) and fatty acid oxidation (Fig. 2H) in the soleus muscle. We also evaluated the interaction between hypothalamic ERK1/2 signaling and lipid metabolism in the skeletal muscle of humans. The interaction and heatmap graphs confirmed a consistent association between hypothalamic *ERK1* and *ERK2* gene expression and several genes involved in fatty acid metabolism in human skeletal muscle (Fig. 2, I to K), but not glucose metabolism or protein synthesis (Fig. 2I). Together, bioinformatics and experimental data demonstrated that the hypothalamic IL6/ERK axis controls AMPK/ACC signaling and fatty acid oxidation in the soleus muscle.

Hypothalamic IL6 stimulates the adrenergic signaling toward the skeletal muscle

Next, we investigated the involvement of the sympathetic nervous system in this neuromuscular circuit. It has been shown that hypothalamic ERK signaling plays a critical role in controlling sympathetic flow (*23*, *24*). The in silico analysis confirmed that hypothalamic *IL6* gene expression is strongly associated with firing rate–related transcripts in mice and humans (fig. S2, B and C). Next, the denervation experiment was performed. The left hindlimb of mice was denervated, and the contralateral paw was used as control. Two days after surgeries (cannula implant and denervation), the animals received mouse recombinant IL6 (200 ng) intracerebroventricular

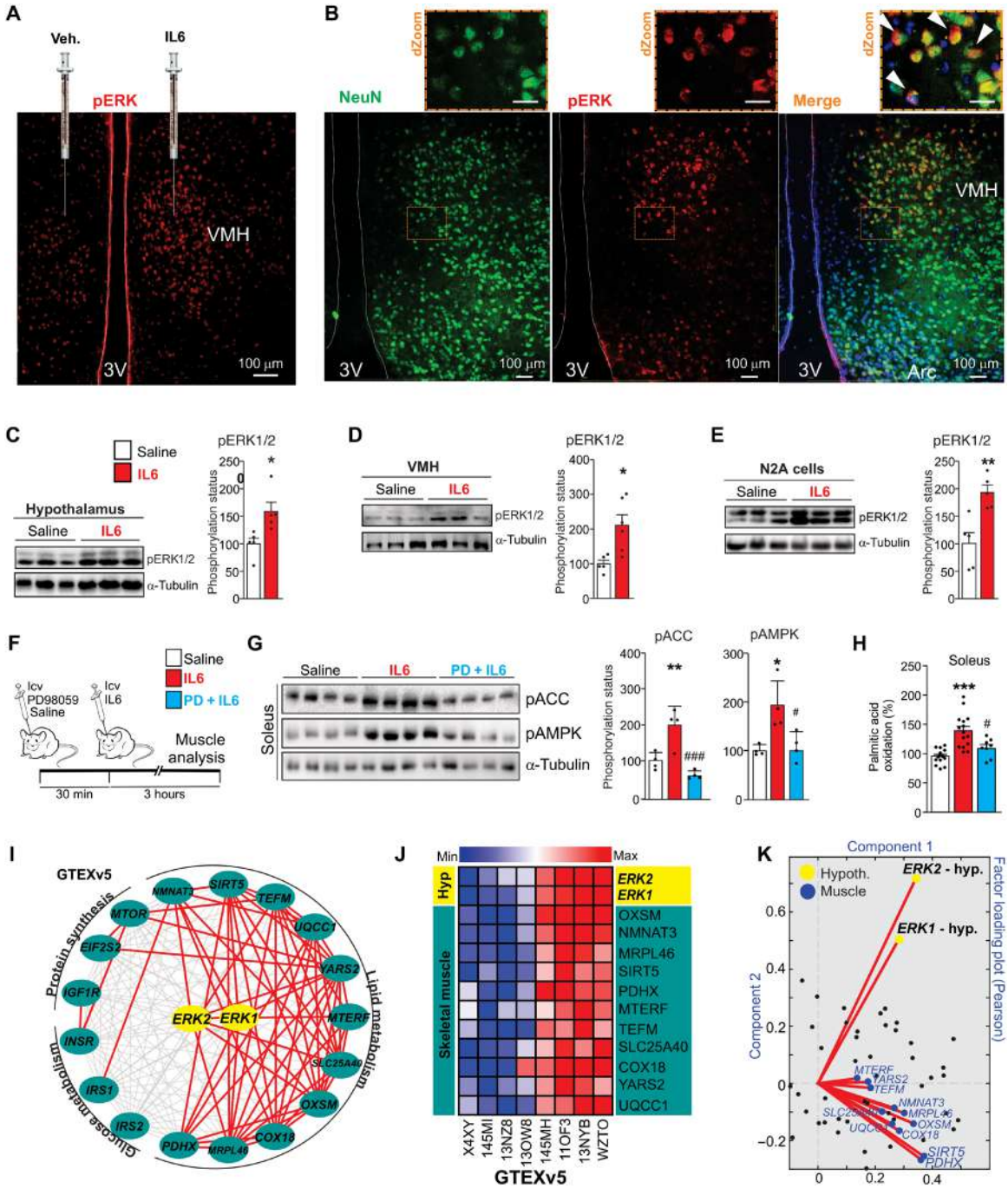

Fig. 2. Evaluation of hypothalamic IL6/ERK axis. (**A**) Phospho-ERK1/2$^{Thr202/Tyr204}$ (pERK1/2$^{Thr202/Tyr204}$) staining in VMH 30 min after vehicle or recombinant IL6 injections. Scale bar, 100 μm. (**B**) pERK1/2 (red) staining in neurons (green) in VMH ($n = 4$). Scale bars, 100 μm. Top panels, digital zoom (dZoom). White arrowheads indicate double staining. Scale bars, 10 μm. (**C**) pERK1/2$^{Thr202/Tyr204}$ 30 min after recombinant IL6 intracerebroventricular microinjection (200 ng) in the whole hypothalamus ($n = 5$) and (**D**) in the ventromedial nucleus ($n = 5$ to 6). (**E**) pERK1/2$^{Thr202/Tyr204}$ in N2A cells after recombinant IL6 incubation (50 ng/ml) for 60 min ($n = 5$). (**F**) Schematic view of the experiment. (**G**) ACC^{Ser79} and AMPK^{Thr172} phosphorylation in the soleus muscle ($n = 4$). (**H**) Palmitic acid oxidation in the soleus muscle ($n = 8$ to 15). (**I**) Interaction and (**J**) heatmap graphs show the positive correlation between hypothalamic *ERK1/2* gene expression and genes related to lipid, glucose, and protein metabolism in the skeletal muscle of humans. Pearson's $r \geq |0.35|$ and $P < 0.05$. $n = 81$. (**K**) Factor loading plot shows that hypothalamic *ERK1/2* gene expressions positively correlate with genes related to fatty acid oxidation in the human muscle as seen on a factor loading plot, where angles less than 90° between gene vectors represent a positive correlation. Unpaired *t* test was used in (C) to (E). One-way ANOVA was used for statistical analysis in (G) and (H). $^{*}P < 0.05$, $^{**}P < 0.01$, and $^{***}P < 0.001$ versus saline and $^{\#}P < 0.05$ and $^{\#\#\#}P < 0.001$ versus IL6.

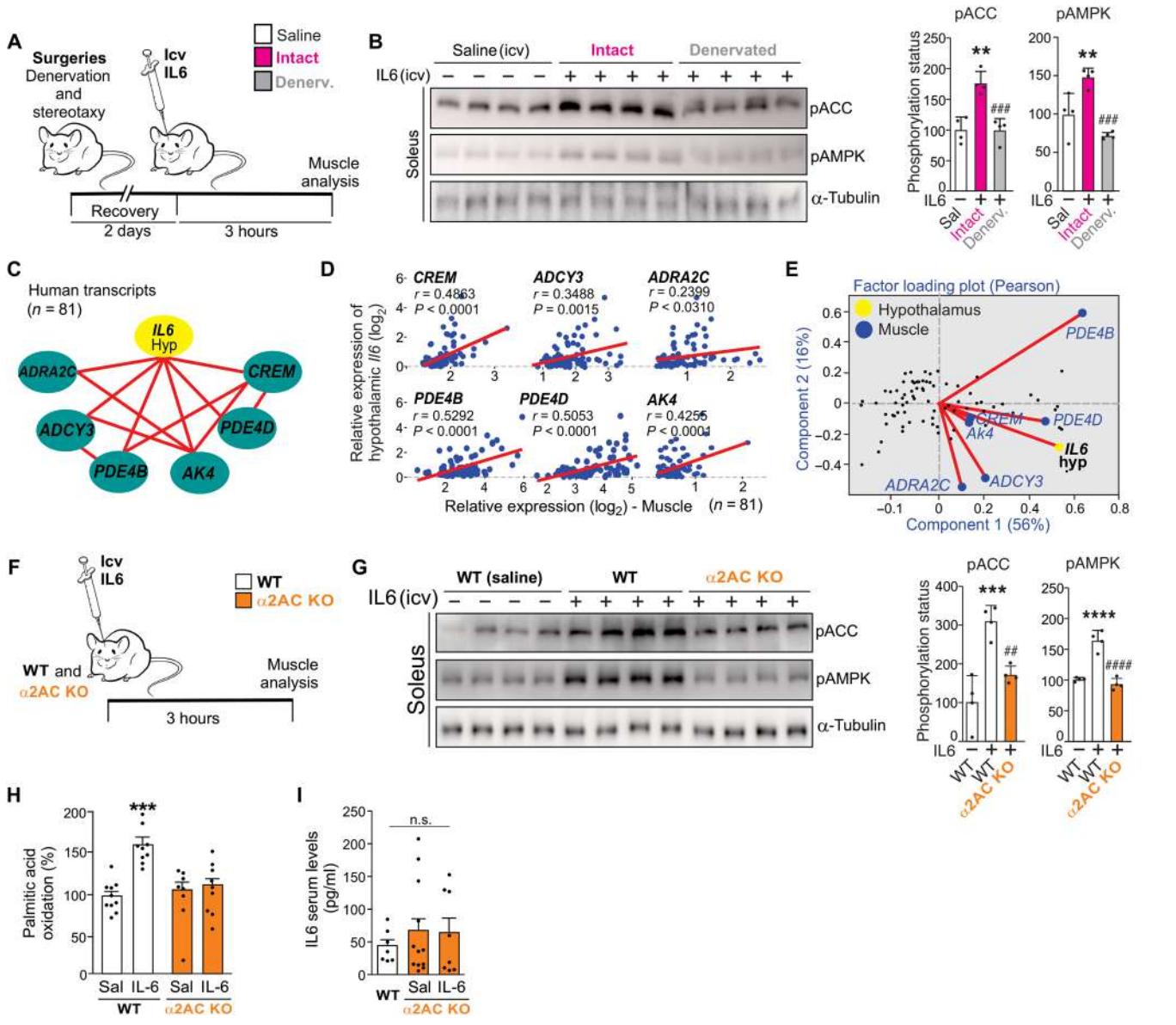

Fig. 3. Evaluation of α2A/α2C adrenoceptor on fatty acid oxidation in muscle. (**A**) Experimental design. Denervation (sciatic nerve) and cannula implantation in the third ventricle were performed on the same procedure day. (**B**) Western blot shows ACC^{Ser79} and AMPK^{Thr172} phosphorylation in the soleus muscle 3 hours after intracerebroventricular infusion of recombinant IL6 (200 ng) ($n = 4$, $^{**}P < 0.01$ versus saline and $^{###}P < 0.001$ versus intact + IL6). (**C**) The interaction graph shows the positive correlation (red lines) between hypothalamic *IL6* gene expression and the gene set related to α-adrenergic signaling in the muscle of humans. (**D**) Pearson's correlation was performed using GTEXv5 human brain hypothalamus Refseq (Sep 15) RPKM $\log_2$ and GTEXv5 human muscle-skeletal Refseq (Sep 15) RPKM $\log_2$ datasets. Red lines represent positive correlation ($n = 81$). (**E**) Factor loading plot (biplot) using the same datasets. (**F**) Wild-type (WT) and male α2A/α2C KO were intracerebroventricularly injected with recombinant IL6, and 3 hours later, the skeletal muscle was examined. (**G**) Western blot shows ACC^{Ser79} and AMPK^{Thr172} phosphorylation in the soleus muscle 3 hours after intracerebroventricular infusion of recombinant IL6 (200 ng) ($n = 4$, $^{***}P < 0.001$ and $^{****}P < 0.0001$ versus wild type + saline and $^{##}P < 0.01$ and $^{####}P < 0.0001$ versus wild type + IL6). (**H**) Palmitic acid oxidation ($n = 8$ to 10, $^{***}P < 0.001$ versus wild type + saline). (**I**) Serum levels of IL6 ($n = 7$ to 11). One-way ANOVA was used for statistical analysis in (B) and (G) to (I).

microinjection, and the soleus muscles were removed, as demonstrated in the experimental design (Fig. 3A). The surgical denervation reduced the ability of the central action of IL6 to phosphorylate ACC and AMPK in the soleus muscle of mice (Fig. 3B), demonstrating that the hypothalamic IL6 requires an intact autonomic nervous system to alter muscle metabolism.

Notably, α-adrenergic signals mediate the ACC phosphorylation and fatty acid oxidation in the skeletal muscle in response to intrahypothalamic injections of leptin (*9*) or the synthetic inhibitor of fatty acid synthase C75 (*25*). On the basis of this information, we sought to determine the involvement of α-adrenergic signaling in this neuromuscular circuit. The interaction graph revealed that the hypothalamic *IL6* gene is positively correlated with the expression of gene set linked to α-adrenergic signaling in the skeletal muscle of humans, including *ADRA2C*, *CREM*, *ADCY3*, *PDE4B*, *PDE4D*, and *AK4* genes (Fig. 3C). These data were also confirmed by

Pearson's correlations (Fig. 3D) and two-component analysis (Fig. 3E). In the BXD cohort, we found that α2 adrenoceptor subunits (*Adra2c*, *Adra2a*, and *Adra2b*), but not α1 subunits, were highly expressed in the skeletal muscle of strains with high expression of hypothalamic *Il6* gene expression (fig. S3, A to C).

To investigate whether α2 adrenoceptor subunits are involved in the control of muscle metabolism upon intrahypothalamic IL6 infusion, mice lacking both α2A and α2C adrenoceptors [α2AC knockout (KO)] were generated. Wild-type and α2AC KO mice received an intracerebroventricular microinjection of recombinant IL6, and the soleus muscles were removed 3 hours later for analyses (Fig. 3F). The central microinjection of recombinant IL6 stimulated ACC and AMPK phosphorylation in the muscles of wild-type, but not α2AC double KO, mice (Fig. 3G). Furthermore, recombinant IL6 intracerebroventricular administration failed to stimulate fatty acid oxidation in the skeletal muscle of α2AC KO mice (Fig. 3H). There was no difference in the IL6 serum levels between wild-type and α2AC KO mice or after intracerebroventricular IL6 microinjection (Fig. 3I). Together, these data demonstrate that α2A and α2C receptor subunits are involved in the terminal sympathetic flow in muscle fibers, integrating the peripheral actions of hypothalamic IL6.

Exercise stimulates central IL6 production and hypothalamic ERK activation and induces prolonged fatty acid oxidation in the skeletal muscle

After that, we sought to evaluate this neuromuscular circuit under physiological conditions. It has been demonstrated that a single bout of exercise can underpin subsequent resting lipid oxidation for many hours in humans (*26*–*28*). Intriguingly, high levels of IL6 were observed in the hypothalamus of exercised fish (*29*) and mice (*14*), and IL6 is also produced in the central nervous system of humans in response to exercise (*30*). Thus, we monitored the contribution of this neuromuscular mechanism in the control of fatty acid oxidation in the skeletal muscle after exercise.

We evaluated the central and peripheral IL6 production and fatty acid metabolism in the skeletal muscle after the acute swimming protocol, as illustrated (Fig. 4A). High levels of *Il6* mRNA were found in the hypothalamus immediately (0 hours) after the acute

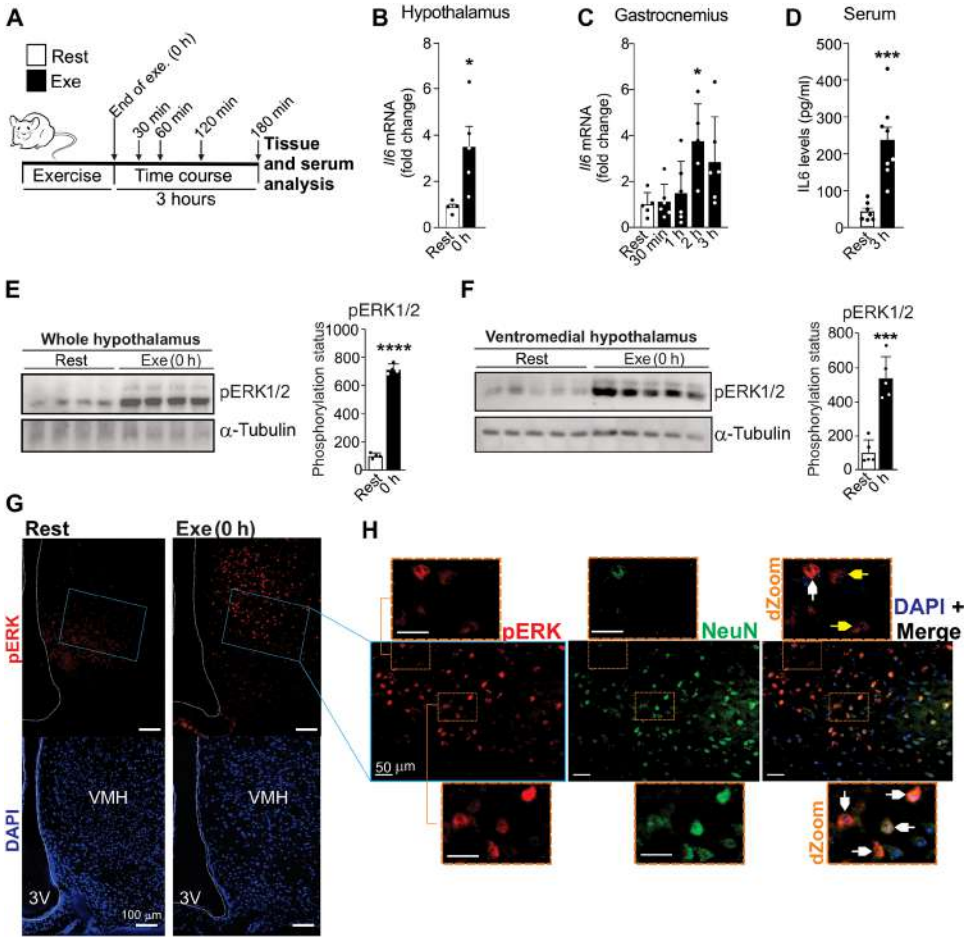

Fig. 4. Exercise stimulates hypothalamic IL6/ERK axis. (**A**) Experimental design. (**B**) Hypothalamic *Il6* gene expression immediately after the exercise protocol ($n = 5$, $^*P < 0.05$ versus Rest). (**C**) *Il6* gene expression in the gastrocnemius muscle after the exercise protocol ($n = 5$ to 6, $^*P < 0.05$ versus Rest). (**D**) Serum levels of IL6 ($n = 7$ to 8, $^{***}P < 0.001$ versus Rest). pERK1/2$^{Thr202/Tyr204}$ in (**E**) hypothalamus ($n = 4$) and (**F**) VMH ($n = 5$). (**G**) pERK staining (red) in VMH of mice ($n = 4$). Scale bars, 100 μm. (**H**) pERK (red) and NeuN (green) double staining in VMH of exercised mice ($n = 5$). Scale bars, 50 μm. dZoom from the orange rectangles highlighting double staining in neuronal (white arrows) and nonneuronal cells (yellow arrows) ($n = 5$). Scale bars, 10 μm. Unpaired *t* test was used in (B) and (D) to (F). One-way ANOVA was used for statistical analysis in (C). $^*P < 0.05$, $^{***}P < 0.001$, and $^{****}P < 0.0001$ versus Rest.

exercise (Fig. 4B). However, no difference was found in other brain regions, such as the hippocampus and cortex (around the parietal region) (fig. S4, A and B). In addition, acute exercise did not change *Il6ra* gene expression in the hypothalamus (fig. S4C).

This swimming protocol showed that peripheral IL6 was produced later in comparison to hypothalamus, given that the *Il6* mRNA in the gastrocnemius muscle was significantly increased 120 min (2 hours) after the acute exercise (Fig. 4C). No difference was found in *Il6* mRNA levels in the soleus muscle of exercised mice (fig. S4D). No changes were found in IL6 serum levels in the first 2 hours after the exercise protocol (fig. S4E). IL6 serum levels were significantly detected 3 hours after the exercise (Fig. 4D).

Consistent with the hypothalamic IL6 production in response to exercise, ERK1/2$^{Thr202/Tyr204}$ phosphorylation was also increased immediately after exercise in the hypothalamic tissue (Fig. 4E), including in VMH (Fig. 4F). Immunofluorescence assay confirmed the presence of ERK1/2$^{Thr202/Tyr204}$ phosphorylation in VMH of exercised, but not control, mice (Fig. 4G). Furthermore, several positive pERK cells were found in neurons of VMH in exercised mice, as indicated by white arrows (Fig. 4H). We also detected the presence of pERK-positive cells in nonneuronal cells of VMH in response to exercise, as indicated by yellow arrows (Fig. 4H).

In terms of fatty acid metabolism in the skeletal muscle in response to exercise, AMPK and ACC phosphorylation were still increased in the soleus muscle 3 hours after exercise (fig. S4F). RNA sequencing analysis was performed to confirm the presence of the oxidative profile in the skeletal muscle 3 hours after the acute exercise. Several genes involved in the mitochondrial function, lipid metabolism, and adrenergic signaling were up-regulated (fig. S4G), whereas, among 99 genes that were up-regulated in response to exercise, almost half of these genes are related to the mitochondrial activity (24 genes), lipid metabolism (15 genes), and adrenergic signaling (7 genes) (fig. S4, G and H).

Swimming exercise protocols are typically used as stressful stimulus for mice (*31*). IL6-null mice (IL6KO) were submitted to the same swimming exercise protocol to address the interference of swimming-induced stress in this neuromuscular mechanism. In contrast to wild-type mice, the swimming exercise protocol failed to stimulate ERK1/2 phosphorylation in the hypothalamus and flopped to sustain ACC and AMPK phosphorylation 3 hours after exercise in the muscle of IL6KO mice (fig. S5, B and C), confirming that endogenous IL6 levels, but not stress-associated factors, are required to elicit this neuromuscular response. Beyond the swimming exercise, we also monitored the central levels of IL6 and AMPK phosphorylation after a moderate-intensity acute treadmill running protocol (fig. S5D). Like the swimming exercise, treadmill running increased hypothalamic IL6 accumulation (fig. S5E) and induced prolonged AMPK phosphorylation in the soleus muscle (fig. S5F), reinforcing the activation of this neuromuscular system under different exercise models. These data collectively demonstrated that the hypothalamic IL6/ERK axis plays a critical role in controlling muscle metabolism under physiological conditions.

Hypothalamic IL6 controls muscle fatty acid oxidation after exercise

To explore the relevance of IL6 action specifically in the hypothalamus, exercised mice received anti–IL6 antibody (IL6 AB) intracerebroventricular microinjections 30 min before and immediately after the exercise session, and the muscle samples were analyzed 3 hours later, as illustrated in the experimental design (fig. S6A). This experiment revealed that anti–IL6 AB intracerebroventricular microinjections abolished fatty acid oxidation after exercise in the skeletal muscle (fig. S6B).

We confirmed these preliminary findings by using a versatile tool for genome editing, targeting IL6R specifically in VMH of mice using lentiviral vector [short hairpin RNA (shRNA)] microinjection. Five distinct lentivirus clones targeting the hypothalamic IL6R were tested. The TRCN94 lentivirus was the most efficient, reducing hypothalamic IL6R protein content by approximately 40% compared to a nontarget scramble vector (fig. S7A). Next, bilateral microinjections of TRCN94 were then performed to deliver IL6R lentivirus specifically in VMH (IL6R KD^{VMH}). Three days after the lentivirus transduction, food consumption was normalized, and no difference was found in food intake between scramble and IL6R KD^{VMH} mice (fig. S7B). We confirmed that this lentiviral transduction was restricted to VMH, reducing the IL6R content in VMH without affecting the presence of this receptor in adjacent hypothalamic nuclei, including in the arcuate nucleus (Fig. 5, A to D). Seven days after lentivirus microinjection in VMH, the animals were submitted to an acute exercise session. The double-staining assay revealed the abundance of pERK1/2-positive cells in neuronal cells of VMH in the scramble group submitted to acute exercise (Fig. 5E, second panel). However, exercise did not promote the same effect in IL6R KD^{VMH} mice (Fig. 5E, last panel). Quantitative analysis considering pERK1/2-positive cells in neuronal and nonneuronal cells restricted to VMH demonstrated that, while exercise increased pERK1/2-positive cells in hypothalamic cells of scramble group, very few positive cells were found in VMH of IL6R KD^{VMH} exercised mice (Fig. 5F).

High levels of AMPK and ACC phosphorylation were observed 3 hours after exercise in the soleus muscle of control (scramble), but not IL6R KD^{VMH}, mice (Fig. 5G). Last, mass spectrometry analysis was performed 3 hours after the exercise protocol and confirmed that exercise markedly reduced the amount of fraction of saturated, monounsaturated, and polyunsaturated fatty acid fractions in the skeletal muscle of control (scramble), but not IL6R KD^{VMH}, mice (Fig. 5, H to J, and fig. S7C).

Together, our findings demonstrate that the hypothalamic IL6/ERK axis in VMH drives fatty acid metabolism in the skeletal muscle (fig. S7D), and this neuromuscular circuit seems to be critical to underpin fatty acid oxidation in the skeletal muscle after exercise.

DISCUSSION

We reported that hypothalamic IL6/ERK signaling induces fatty acid oxidation in the skeletal muscle. We demonstrated that ERK signaling in VMH mediates IL6-induced AMPK and ACC phosphorylation and fatty acid oxidation in oxidative muscles. Evidence for the involvement of the α-adrenergic system in the connection of the central action of IL6/ERK signaling to fatty acid metabolism in the skeletal muscle was reported. Notably, we demonstrated that α2A and α2C receptors play a crucial role in this physiological mechanism (fig. S7D). The physiological relevance of these findings was observed in fatty acid metabolism in the skeletal muscle after exercise.

Several studies have demonstrated that the central or peripheral action of IL6 controls energy expenditure and lipid metabolism in animals and humans (*13*, *32*–*34*). Wallenius and colleagues (*13*) reported that central, but not peripheral, IL6 injection increased energy expenditure in mice. Moreover, the microinjection of recombinant

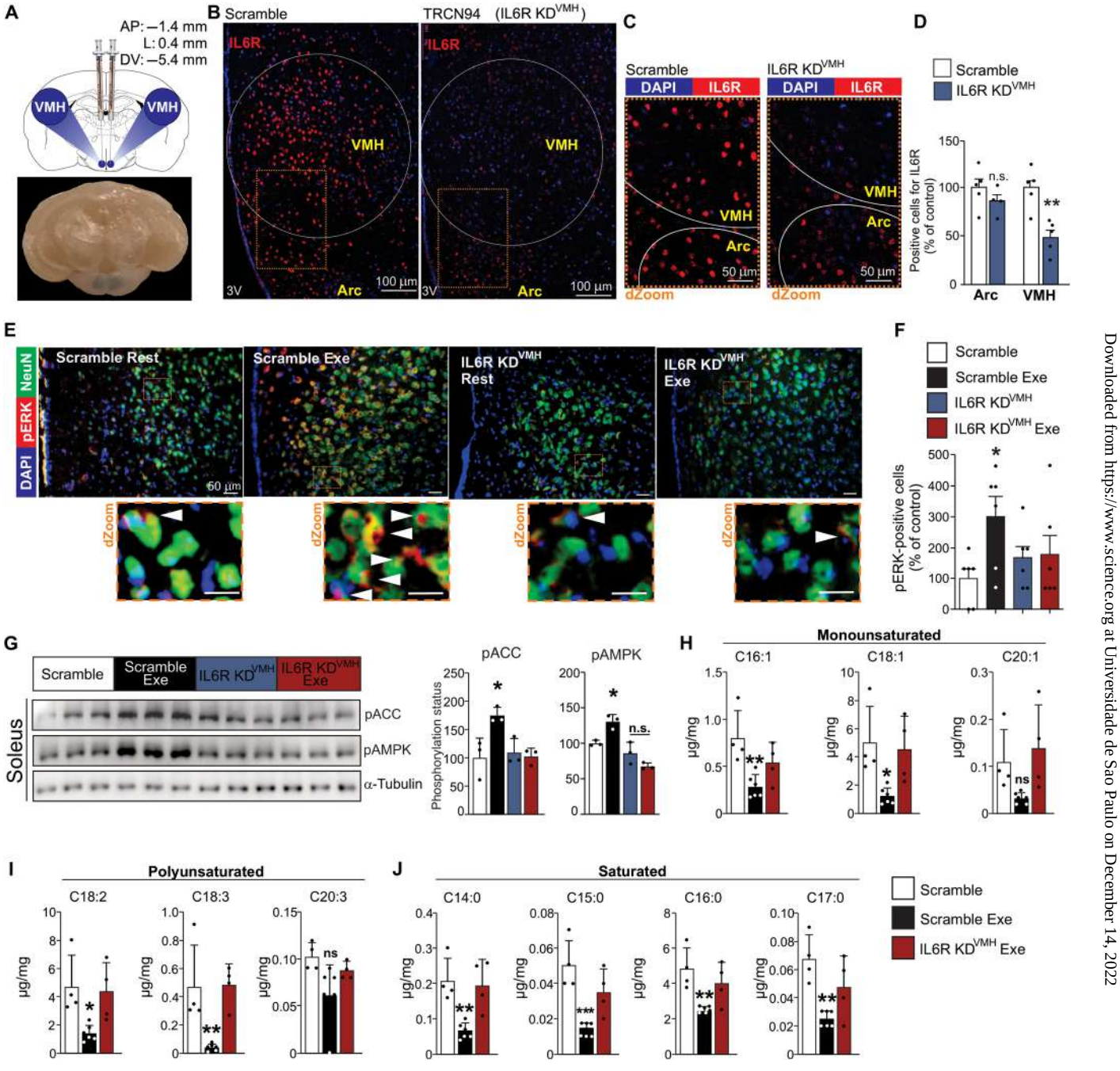

Fig. 5. Hypothalamic IL6 controls muscle fatty acid oxidation after exercise in mice. (**A**) Illustration for VMH microinjections and a representative picture of a coronal view of a mouse brain, demonstrating the blue dye staining confirming the anatomical localization of bilateral microinjections in VMH (bottom). KD, knockdown. (**B**) IL6R (red) in the arcuate nucleus and VMH 7 days after VMH lentivirus injection ($n = 5$ to 6). Scale bars, 100 μm. (**C**) dZoom from the orange rectangles highlighted in (B) shows the presence of IL6R (red). Scale bars, 50 μm. DAPI, 4′,6-diamidino-2-phenylindole. (**D**) IL6R-positive cells in the arcuate and ventromedial nuclei ($n = 5$ to 6, $^{**}P < 0.01$ versus scramble). (**E**) Top panels: Colocalization of ERK1/2 phosphorylation (red) in neurons (green) of VMH ($n = 3$ to 5). Scale bars, 50 μm. Bottom panels: dZoom from the orange rectangles highlighted in the top panels shows the presence of pERK1/2 in neuronal cells. Scale bars, 10 μm. (**F**) Positive cells for pERK1/2 in neuronal and nonneuronal cells in VMH of mice ($n = 6$, $^{*}P < 0.05$ versus scramble at rest). (**G**) ACC and AMPK phosphorylation in the soleus muscle ($n = 3$, $^{*}P < 0.05$ versus scramble at rest). (**H** to **J**) Determination of fatty acid fractions in the gastrocnemius muscle ($n = 4$ to 6). Unpaired *t* test was used in (D) and (F). One-way ANOVA was used for statistical analysis in (G) and (H).

IL6 into the lateral cerebral ventricle increased the body temperature in rats (*35*). The IL6-deficient mouse displayed lower oxygen consumption during exercise (*36*). The present study demonstrated that recombinant IL6 intracerebroventricular injection increased oxygen consumption and fatty acid oxidation in the soleus muscle of mice. These findings collectively illustrate the critical role of the central IL6 in the control of energy homeostasis and peripheral metabolism.

VMH neurons have been extensively associated with skeletal muscle metabolism. For instance, the central action of orexin A in VMH induced glucose uptake in the skeletal muscle of mice (*7*). The stimulation of the hypothalamic ERK1/2 pathway has also been involved in controlling glucose metabolism in the skeletal muscle. ERK and its upstream kinase MEK regulate the leptin-induced increase in glucose uptake and insulin sensitivity in oxidative fibers in the skeletal muscle of mice through activation of the melanocortin system in VMH (*20*). Our study demonstrated that specific ERK1/2 activation in VMH through the IL6 action induced AMPK and ACC phosphorylation and fatty acid oxidation in the soleus muscle of mice. Beyond VMH, IL6 also plays a critical role in controlling metabolism by acting in other hypothalamic nuclei. For example, in the arcuate nucleus, IL6 action is associated with adiposity control in mice (*37*). Moreover, IL6 activity in the paraventricular nucleus (PVN) induces several beneficial metabolic effects even under conditions of leptin resistance (*10*). These studies strongly suggest that hypothalamic IL6 controls various metabolic effects by acting in specific hypothalamic nuclei.

In our study, we found that physical exercise stimulated ERK phosphorylation in neuronal and nonneuronal cells in the hypothalamus of mice. Consistent with these data, positive pERK neurons were detected in different hypothalamic nuclei of wild-type, but not IL6-deficient, mice after a stressful stimulus (*38*). These data establish that hypothalamic IL6/ERK signaling activation can be observed in different physiological conditions. However, it is essential to mention that IL6 can induce ERK1/2 phosphorylation of neuronal cells through IL6 trans-signaling (*21*, *22*). The IL6 trans-signaling pathway occurs when the IL6 and soluble IL6R (sIL6R) complex (IL6/sIL6R) activates glycoprotein 130 (gp130) (*39*). IL6 trans-signaling mediates several metabolic effects of IL6 in peripheral tissues and the central nervous system (*10*, *39*). For instance, Timper and colleagues (*10*) reported that IL6 controls energy and glucose homeostasis through gp130 expression in the PVN of obese animals, independently of IL6R. However, the role of IL6 trans-signaling was not monitored in the present study.

Hormonal and neural factors mediate the interaction between the central nervous system and muscle metabolism and function. In this context, the sympathetic outflow plays an essential role in the control of the activity of peripheral tissues, such as adipose and hepatic tissue and skeletal muscle (*7*, *40*, *41*). It has been shown that denervation of the sciatic, femoral, and obturator nerves abolishes the increase in AMPK phosphorylation in the skeletal muscle observed in intracerebroventricular leptin-injected mice (*9*). Our results demonstrated that the hypothalamic IL6/ERK axis induced fatty acid oxidation in the skeletal muscle through sympathetic outflow and the α2-adrenergic pathway, involving the α2A and α2C receptors. These findings agree with results reported by others since the stimulation of the α-adrenergic pathway, but not the β-adrenergic pathway, is involved in AMPK activation in the skeletal muscle (*9*). However, the precise mechanism by which α2A and α2C receptors induce AMPK and ACC phosphorylation in the skeletal muscle is unclear.

We and others previously demonstrated that acute exercise promoted a prolonged AMPK and ACC phosphorylation in the skeletal muscle of rodents (*42*–*44*). Similar data were found in different studies involving exercised humans (*45*–*47*). In addition, a single bout of exercise can underpin subsequent resting lipid oxidation for many hours in humans (*26*–*28*). These findings seem to be strongly associated with the physiological phenomenon informally called "afterburn." Human studies showed that AMPK/ACC signaling remained activated in the skeletal muscle for 60 and 120 min (*47*, *48*). Our results demonstrated that both IL6 intracerebroventricular injection and exercise increase AMPK and ACC phosphorylation and fatty acid oxidation in the skeletal muscle of mice up to 3 hours afterward. Curiously, tocilizumab, an IL6R blocker, induces abnormal lipid metabolism accumulation and disrupts fatty acid mobilization in the adipose tissue of lean and obese exercised subjects (*49*, *50*). Together with our findings, these data demonstrate that targeting IL6 signaling may disturb the lipid metabolism affecting metabolic health.

Previously, we demonstrated that different types of acute exercise, such as swimming and treadmill running, increased the *Il6* mRNA levels in the hypothalamus of mice (*14*) Similarly, stress protocols up-regulated *Il6* mRNA expression in rat hypothalamus (*38*, *51*). In addition, a high capacity of hypothalamic microglial cells of mice to produce IL6 under several acute or chronic circumstances has been demonstrated (*52*). Furthermore, human brain IL6 production was confirmed after acute prolonged exercise (*30*). Collectively, these studies strongly suggest the ability of hypothalamic cells to produce IL6 under physiological and pathophysiological conditions. Regarding the source of IL6 in exercised mice, a time-course study revealed the rapid accumulation of *Il6* mRNA in the hypothalamus, confirming the ability of hypothalamic cells to produce IL6 in response to exercise. Recently, an interesting study using in situ hybridization method reported that IL6 could be produced in neurons, astrocytes, and microglia in the lateral parabrachial nucleus of mice (*12*). In the present study, we demonstrated that exercise rapidly increased *Il6* mRNA levels in the hypothalamus and stimulated ERK phosphorylation in neuronal and nonneuronal cells; however, we did not assess which cell type is responsible for the hypothalamic production of IL6 in response to exercise. In addition, beyond the central production, we may consider that muscle-derived IL6 can also reach the central nervous system.

Last, our study demonstrated that the hypothalamic IL6/ERK axis increases AMPK and ACC phosphorylation and stimulates fatty acid oxidation in the skeletal muscle. Pharmacological, physiological, and genetic approaches revealed that the α-adrenergic system mediates the communication between the hypothalamic IL6/ERK1/2 axis and AMPK/ACC signaling in the muscle. The findings point out that the reported neuromuscular circuit plays an important role in regulating fatty acid metabolism in the skeletal muscle.

MATERIALS AND METHODS

N2A cells

N2A cells, derived from mouse neurons, were cultivated in Dulbecco's modified Eagle's medium (DMEM)/HamF12 (1:1) supplemented with 10% (v/v) fetal bovine serum (FBS) and streptomycin/penicillin (100 U/ml). Cells were cultivated at 37°C in a humidified atmosphere containing 5% CO_2. N2A cells were subjected to neurite differentiation before treatments by incubation with medium containing

2% FBS for 24 hours. Cells were treated with IL6 (50 ng/ml) for 60 min. For protein extraction, cells were resuspended in lysis buffer [50 mM tris-HCl (pH 7.4), 150 mM NaCl, 1 mM EDTA, and 1% Triton X-100] containing protease and phosphatase inhibitor cocktails (Roche). Lysates were incubated on ice for 15 min and centrifuged at 12,000*g* for 10 min at 4°C. Supernatants were collected and stored for immunoblotting analysis.

Animals

C57BL6/J, IL6KO mice, and α2A/α2C adrenoceptor KO (α2AC KO) male mice were used. C57BL6/J mice were obtained from the University of Campinas Central Breeding Center. IL6-KO, TLR4KO, and α2AC KO were from the University of São Paulo. Male wild-type and congenic α2A/α2C KO (*53*) mice with C57BL6/J genetic backgrounds were from the University of São Paulo.

Mice were kept in individual cages with controlled temperature (22° to 24°C) and light and dark cycles (12 hours). Lights were turned on at 6 a.m. and turned off at 6 p.m. They had ad libitum access to standard rodent chow (Quimtia, Nuvilab) and water. All experimental protocols were subjected to the University of Campinas Animal Ethics Use Committee (#2849-1 and #4563-1/2017). The number of animals used in each experiment was described in the figure legends.

Physical exercise protocols

Swimming exercise

Four animals per turn were acclimated to the water for three consecutive days, 10 min a day, in plastic containers of 40 cm in length, 30 cm in width, and 45 cm in depth. The water temperature was maintained at approximately 33°C during the entire protocol. Afterward, part of the acclimated animals was subjected to a single bout of exercise. The swimming protocol was composed of four sessions of 30 min with 5-min intervals in between, for a total of 2 hours, as previously described (*14*).

Treadmill running

Five animals were acclimated to treadmill apparatus for five consecutive days, 10 min/day, 10 m/min without inclination. Next, the incremental load test was performed to determine the exhaustion velocity, as previously described (*54*). Forty-eight hours later, the animals performed an acute exercise that consisted of two sessions of 60 min at 60% of exhaustion velocity, separated by 20 min of interval.

Serum IL6 determination

IL6 serum levels were determined using an enzyme-linked immunosorbent assay (ELISA) kit (Pierce Endogen, Rockford, IL), following the manufacturer's recommendations.

Cannula implantation

Animals were anesthetized with ketamine (100 mg) and diazepam (0.07 mg) (0.2 ml/100 g body weight). The procedure started when corneal and paw pain reflexes were abolished. Animals were positioned at the stereotaxic coordinates, and a 1-cm intraparietal incision was performed after cranial trichotomy and antisepsis. Afterward, the periosteum was divulsed, and with the exposed skullcap, the bregma was visualized for the stereotaxic coordinates. Cannula implantation was aimed at the third ventricle of mice weighing 25 to 30 g [coordinates: AP (antero-posterior): −1.8 mm, L (lateral): 0.0 mm, DV (dorsoventral): −5.0 mm] according to the stereotaxic atlas. After a 1-week recovery period, the positioning of the intracerebroventricular cannula was confirmed by a positive drinking response after administration of angiotensin II (40 ng); animals that did not drink water after angiotensin injection were not included in the experiment.

Intracerebroventricular microinjections

Recombinant IL6

Intracerebroventricular IL6 mouse recombinant microinjection (200 ng) from Sino Biological (50136-MNAE) was performed between 5:00 and 6:00 p.m., as previously described (*14*).

IL6 neutralizing antibody

Animals were randomly selected for intracerebroventricular microinjection containing saline or rabbit antiserum against IL6 (IL6 AB). Anti–IL6 AB (100 ng) from Santa Cruz Biotechnology was performed 30 min before and immediately after the exercise protocol, as previously published (*14*).

PD98059

Mice were randomly selected for intracerebroventricular microinjection containing saline or PD98059 (60 μM), a selective, cell-permeable inhibitor of the MEK, as previously described (*55*). PD98059 was performed 30 min before the intracerebroventricular recombinant IL6 microinjection.

VMH IL6R lentivirus transfection

Five different shRNA-based lentiviral clones [The RNAi Consortium (TRC); titer, 10^6] targeting IL6R [TRCN 0000057 (LV1), TRCN 0000059 (LV2), TRCN 0000089 (LV3), TRCN 0000093 (LV4), and TRCN 0000094 (LV5)] or scramble (SHC 016 V, pLKO.1-puro nonmammalian shRNA control) (SCR) from Sigma-Aldrich (St. Louis, MO, USA) were tested for IL6R knockdown in preliminary experiments, as previously described (*56*). Mice were submitted for stereotaxic surgery (Ultra Precise, model 963, Kopf). Lentiviral shRNA particle (LV5) was administered bilaterally (1 μl/min) into VMH following the coordinates: AP, −1.4 mm; L, ±0.4 mm; DV, −5.4 mm. Injection of Evans blue and dissection of the region of interest provided anatomical control of the stereotaxic procedure.

Reagents and antibodies

Reagents for SDS–polyacrylamide gel electrophoresis (SDS-PAGE) and immunoblotting were from Bio-Rad Laboratories (Hercules, CA). Tris, aprotinin, adenosine triphosphate (ATP), dithiothreitol, phenylmethylsulfonyl fluoride, Triton X-100, Tween 20, glycerol, and bovine serum albumin (BSA) (fraction V) were from Sigma Chemical Co. (St. Louis, MO). Nitrocellulose paper (BA85, 0.2 mm) was from Schleicher & Schuell (Keene, NH). Ketamine hydrochloride was from Cristália (Itapira SP, Brazil). The chemiluminescent kit was from Thermo Fisher Scientific (Rockford, IL, USA). The following antibodies were used: Anti-IL6 (M-19) and anti–α-tubulin (B-7) were from Santa Cruz Biotechnology; anti-pERK1/2 (Thr^{202}/Tyr^{204}), anti-p44/42 MAPK (ERK1/2), anti-pACC (Ser^{79}), anti-ACC, anti–pAMPK (Thr^{172}), anti-AMPKα, and anti–α-tubulin were from Cell Signaling Technology. Secondary antibodies were from Thermo Fisher Scientific. Recombinant IL6 was from Calbiochem (San Diego, CA, USA). PD98059 was from LC Laboratory (Woburn, MA). Unless otherwise specified, routine reagents were purchased from Sigma Chemical Co. (St. Louis, MO). The doses administered in each experimental group are given below.

Immunoblotting

After the respective treatments, animals were anesthetized. Samples from the hypothalamus and soleus muscle were obtained, minced

coarsely, and homogenized immediately in solubilization buffer containing 100 mM tris (pH 7.6), 1% Triton X-100, 10 mM Na_3VO_4, 100 mM NaF, 10 mM $Na_4P_2O_7$, 4 mM EDTA, 150 mM NaCl, aprotinin (0.1 mg/ml), and phenylmethylsulfonyl fluoride (35 mg/ml) using a Polytron PTA 20S generator (model PT 10/35, Brinkmann Instruments, Westbury, NY) operated at maximum speed for 30 s and clarified by centrifugation. All the samples from all groups were subjected to SDS-PAGE and blotted onto a nitrocellulose membrane. The membranes were incubated for 12 hours at 4°C with primary antibody after blockade with 5% nonfat milk in tris-buffered saline with Tween 20 (TBST) (10 mM tris, 150 mM NaCl, and 0.02% Tween 20) for 90 min at room temperature. After the secondary antibody incubation, the signal was detected for 60 min in a 3% nonfat milk–TBST solution, treated with 2 ml of SuperSignal West Pico Chemiluminescent Substrate, exposed to photosensitive RX film from Kodak, or visualized using G:Box from SynGene. Band intensities were quantified by optical densitometry using UN-SCAN-IT gel 7.1 (Silk Scientific Inc.). Ponceau staining from Sigma-Aldrich (St. Louis, MO, USA) was also used to monitor the loading control for each sample.

mRNA isolation and real-time PCR

Total RNA was extracted using TRIzol reagent (Life Technologies), according to the manufacturer's recommendations. Total RNA was rendered genomic DNA free by digestion with ribonuclease-free deoxyribonuclease (RQ1, Promega, Madison, WI, USA). Real-time polymerase chain reaction (PCR) and mRNA isolation were performed using a commercial kit (GAPD, 4352338E) for mouse and TaqMan gene expression assays for mouse IL6 (Mn00446190_m1), and using the following primers: *Cpt1*β, 5′-TCGAATCAAGAATGGCATCCT-3′ (forward) and 5′-GAGATGTCCACCTTGCAGTAGTTG-3′ (reverse); *Pparα*, 5′-TTAGAGGAGAGCCAAGTTGAAGTTC-3′ (forward) and 5′-GCAGGCCACAGAGCGCTAA-3′ (reverse); *Il6ra*, 5′-TGCAGTTCCAGCTTCGATACCG-3′ (forward) and 5′-TGCTTCACTCCTCGCAAGGCAT-3′ (reverse).

Oxygen consumption determination

O_2 consumption was measured using an indirect open circuit calorimeter (CLAMS, Oxymax Deluxe System, Columbus Instruments, Columbus, OH, USA). Mice were adapted 1 day before the experiment. Measurements were performed for 3 hours after intracerebroventricular IL6 microinjection.

Palmitate oxidation in soleus muscle

The animals were euthanized, and their soleus muscles were isolated and incubated as previously described (*57*). Briefly, mice were sacrificed by cervical dislocation, and their soleus muscles were carefully and quickly isolated, kept under resting tension with stainless steel clips, and preincubated in a buffered Krebs-Ringer bicarbonate (TBKR) containing 5.6 mM glucose (pH 7.4) for 30 min in a heated bath to 35°C with 95% O_2 and 5% CO_2, with continuous shaking (90 oscillations/min). After this period, the muscles were transferred to other vials containing the same buffer but added with [U-^{14}C]palmitate (0.2 μCi/ml) and 100 μM unlabeled palmitate. The latter was previously diluted in ethanol (80 mM solution) before adding the incubation buffer. NaOH solution (2 M) was added to a microtube isolated from the inside of the bottle to adsorb $^{14}CO_2$. The muscles were incubated for 2 hours under the same conditions. At the end of the incubation, muscles were briefly washed in cold TBKR (4°C), dried on filter paper, frozen in liquid nitrogen, and subsequently weighed. The flasks were hermetically sealed to measure the oxidation of [U-^{14}C]palmitate as previously described (*58*).

Mass spectrometry analysis for fatty acid determination

For fatty acid profile determination, 150 μl of tissue homogenates was taken in a screw cap glass tube containing 25 μg of internal standard (tridecanoic acid, C13:0). After that, 1 ml of 0.5 M NaOH-methanol was added, and the sample was boiled at 100°C for 15 min. After cooling the samples, 2 ml of BF3-methanol was added, and the sample was boiled at 100°C for 20 s. The sample was again cooled to room temperature, and 1 ml of isooctane was added. The tubes were shaken, and 5 ml of saturated NaCl solution was added. After phase separation, the supernatant was collected and evaporated with nitrogen gas to concentrate the fatty acid methyl esters (FAMEs). FAME was resuspended in 50 μl of hexane for chromatographic analysis (*59*). Chromatographic analyses were performed using a gas chromatograph–mass spectrometer (model GCMS-QP2010 Ultra, Shimadzu). A fused silica capillary column (Stabilwax; length, 30 m; internal diameter, 0.25 mm; thickness, 0.25 μm; Restek, USA) was used to inject 1 μl of the sample at 250°C. High-grade pure helium (He) was used as the carrier gas with a constant flow rate of 1.3 ml/min with a split injection of 2:1. The oven temperature was programmed from 80° to 175°C at a rate of 5°C/min, followed by another gradient of 3°C/min to 230°C, which was maintained for 10 min. Mass conditions were as follows: ionization voltage, 70 eV; ion source temperature, 200°C; full scan mode in the mass range of 35 to 500 with a velocity of 0.2 s per scan.

Immunofluorescence staining

Ad libitum–fed animals were perfused with 4% paraformaldehyde transcardially. The brains were immersed in 10% (w/v) sucrose and, after 24 hours, transferred to 30% (w/v) sucrose. After that, they were embedded in optimal cutting temperature (OCT) compound (Sakura Finetek, Torrance, CA) and cut into 20-μm coronal sections using a cryostat. The sections were incubated in blocking solution in PBS (0.2% of Triton X-100) and 5% BSA for 2 hours at 21°C and then incubated overnight at 4°C in mouse anti-NeuN (1:300; Millipore, MAB377), anti-IL6Rα (1:200; Santa Cruz Biotechnology, sc660), anti–phospho-p44/42 MAPK (ERK1/2) (Thr^{202}/Tyr^{204}) (D13.14.4E) XP Rabbit mAb #4370 (Cell Signaling Technology), and anti–SF-1 antibody (A-1; 1:200; Santa Cruz Biotechnology, sc-393592). After washing in PBS, sections were placed in secondary donkey anti-mouse fluorescein isothiocyanate (1:500; Santa Cruz Biotechnology, sc 2010) and goat anti-rabbit Alexa Fluor 546 (1:500; Thermo Fisher Scientific, CA, USA) for 2 hours and mounted with VECTASHIELD Mounting Medium with 4′,6-diamidino-2-phenylindole (DAPI) (#H-1200, Vector Laboratories Inc., Burlingame, CA, USA). The images were acquired with a confocal laser microscope (LSM 780, Zeiss, Jena, Germany). Digital/electronic zoom of highlighted areas was performed when necessary.

Confocal microscopy

Briefly, after fixation with 4% paraformaldehyde, the slides were washed with PBS, then incubated for 10 min with glycine (0.1 M), and treated for 30 min with 4% BSA solution (Sigma-Aldrich). The slides then were incubated overnight at 4°C with a recombinant mouse immunoglobulin G (IgG) antibody against IL6Rα (D-8, sc-274259, Santa Cruz Biotechnology) and a recombinant rabbit IgG

antibody against phospho-p44/42 MAPK (ERK1/2, 4370, Cell Signaling Technology), both diluted in 1% BSA. The slides were washed and incubated for 2 hours with secondary antibodies (Alexa Fluor 488–conjugated, catalog number A32723, Thermo Fisher Scientific, Waltham, MA, USA; Alexa Fluor 594–conjugated donkey anti-rabbit IgG, catalog number A21207, Thermo Fisher Scientific, Waltham, MA, USA) diluted 1:500 in 1% BSA. Cells were washed and stained with DAPI (catalog number SC3598, Santa Cruz Biotechnology, Dallas, TX, USA) for nuclear labeling. Microscopic images were acquired using Zeiss LSM 880 with Airyscan on an Axio Observer 7 inverted microscope (Carl Zeiss, Jena, Germany) with a C Plan-Apochromat 63×/1.4 oil differential interference contrast objective lens with 4× optical zoom. Before visual inspection of the images, raw .czi files were automatically processed into deconvoluted Airyscan images using Zen Black 2.3 software. DAPI staining was visualized with conventional confocal imaging using a 405-nm laser line for excitation and a pinhole set to 1 Airy unit.

Arc and VMH cell counting

Sections from the immunofluorescence assay were used to determine ERK1/2 phosphorylation in VMH of mice transfected with IL6R shRNA (LV5) or scramble. Images were obtained, isolating only Arc or VMH in the images. Five images per group were counted blindly by two independent researchers using ImageJ software 1.48v. The average of each image was used to obtain the group mean.

Hypothalamic VMH dissection

The microdissections were performed according to previous studies (*9*, *60*, *61*). Fresh whole brains were dissected using a specific steel matrix for mouse brains. Slices (1 mm) were cut following the sagittal orientation. The cuts were made using ultrathin blades (6×10^{-5} mm thick), and the first sections from the midline of the brain were used for the microdissection of VMH/DMH (dorsomedial hypothalamus) using a microscope and following the mouse brain atlas coordinates. VMH was quickly frozen in liquid nitrogen for further protein analysis.

Denervation experiment

For the denervation experiments, mice were anesthetized with ketamine (100 mg) and diazepam (0.07 mg) (0.2 ml/100 g body weight). The procedure started when corneal and paw pain reflexes were abolished. Denervation and cannula implantation surgeries were performed in the same procedure. The left hindlimb muscles were carefully denervated by excising approximately 4 mm of the sciatic nerve. The animals were used in the experiment 48 hours later, and the contralateral paw was used as control.

BXD hypothalamus microarray processing

Correlation analyses were performed using hypothalamic mRNAs of the BXD inbred family [Hypothalamus Affy MoGene 1.0 ST (Nov10) and EPFL/LISP BXD CD Muscle Affy Mouse Gene 1.0 ST (Dec11) RMA] (*16*), except for fig. S2B. These datasets are accessible on GeneNetwork (www.genenetwork.org) (*62*). The Pearson's and Spearman's correlation graphs were built using Prism graph, and the heatmap graphs were obtained using the GENE-E software.

For fig. S2B, we downloaded the $\log_2$-transformed, RMA (robust multichip average)-normalized (*63*), rescaling BXD hypothalamus microarray intensity data from the 89 BXD mouse hypothalami from Andreux *et al.* (*16*) from the National Center for Biotechnology Information Gene Expression Omnibus (accession number GSE36674). A complete overview of the data and its preprocessing pipeline can be found at GeneNetwork.org (GN accession ID GN317). These 89 samples come from 50 different murine BXD strains, where tissues from two mice of the same strain and sex were pooled. We regressed these preprocessed gene expressions to select outcome firing rate–related genes on the preprocessed gene expressions of *Il6* through ordinary least squares regression. The *P* values associated with the effect of preprocessed *Il6* expression were corrected with the Benjamini-Hochberg false discovery rate procedure and reported as *q* values.

GTEx hypothalamus normalized gene expression processing

GTEXv5 human brain hypothalamus Refseq (Sep 15) RPKM (reads per kilobase million) $\log_2$ and GTEXv5 human muscle-skeletal Refseq (Sep 15) (*15*) were used, except for fig. S2C. These datasets are accessible on GeneNetwork (http://www.genenetwork.org). The Pearson's and Spearman's correlation graphs were built using Prism graph, and the heatmap graph was obtained using the GENE-E software. For fig. S2C, we accessed the normalized, log-transformed (with offset 1) RNA sequencing gene read counts in the hypothalami of 170 deceased human subjects from the GTEx project (*15*) version 8 through accession number dbGaP phs000424.v8.p2 (see www.gtexportal.org/home/documentationPage for a complete overview of the data and its processing pipeline). We regressed these preprocessed gene expressions in GTEx hypothalamus for the human homologs of the firing rate–related genes on the *IL6* preprocessed gene expressions through ordinary least squares regression. The *P* values associated with *IL6* expression were corrected with the Benjamini-Hochberg false discovery rate procedure and reported as *q* values. All individual values used in bioinformatics analysis are described in supplementary tables.

Statistical analysis

The results were expressed as means ± SD. Immunoblot results were presented as direct comparisons between the groups. Data were analyzed by Student's *t* test or one-way analysis of variance (ANOVA), as appropriate, with post hoc Bonferroni or Tukey tests for multiple unpairwise comparisons of the means. The level of significance adopted was $P < 0.05$. Statistica 6.0 software was used for the analysis. Pearson's and Spearman's correlations were used for the bioinformatics analysis, and *r* and *P* values are described in the figures or figure legends. The number of animals/samples used in each experiment is described in the figure legends.

SUPPLEMENTARY MATERIALS

Supplementary material for this article is available at https://science.org/doi/10.1126/sciadv.abm7355

View/request a protocol for this paper from *Bio-protocol*.

REFERENCES AND NOTES

1. C. Cavadas, C. A. Aveleira, G. F. P. Souza, L. A. Velloso, *The Pathophysiology of Defective Proteostasis in the Hypothalamus—From Obesity to Ageing* (Nature Publishing Group, 2016), vol. 12.
2. K. Timper, J. C. Brüning, Hypothalamic circuits regulating appetite and energy homeostasis: Pathways to obesity. *Dis. Model Mech.* **10**, 679–689 (2017).
3. E. Kwon, H.-Y. Joung, S.-M. Liu, S. C. C. Chua, G. J. Schwartz, Y.-H. Jo, Optogenetic stimulation of the liver-projecting melanocortinergic pathway promotes hepatic glucose production. *Nat. Commun.* **11**, 6295 (2020).
4. A. G. Gómez-Valadés, M. Pozo, L. Varela, M. B. Boudjadja, S. Ramírez, I. Chivite, E. Eyre, R. Haddad-Tóvolli, A. Obri, M. Milà-Guasch, J. Altirriba, M. Schneeberger, M. Imbernón,

A. R. Garcia-Rendueles, P. Gama-Perez, J. Rojo-Ruiz, B. Rácz, M. T. Alonso, R. Gomis, A. Zorzano, G. D'Agostino, C. V. Alvarez, R. Nogueiras, P. M. Garcia-Roves, T. L. Horvath, M. Claret, Mitochondrial cristae-remodeling protein OPA1 in POMC neurons couples Ca^{2+} homeostasis with adipose tissue lipolysis. *Cell Metab.* **33**, 1820–1835.e9 (2021).
5. X. Xiao, G. Yeghiazaryan, S. Hess, P. Klemm, A. Sieben, A. Kleinridders, D. A. Morgan, F. T. Wunderlich, K. Rahmouni, D. Kong, T. E. Scammell, B. B. Lowell, P. Kloppenburg, J. C. Brüning, A. C. Hausen, Orexin receptors 1 and 2 in serotonergic neurons differentially regulate peripheral glucose metabolism in obesity. *Nat. Commun.* **12**, 5249 (2021).
6. M. López, L. Varela, M. J. Vázquez, S. Rodríguez-Cuenca, C. R. González, V. R. Velagapudi, D. A. Morgan, E. Schoenmakers, K. Agassandian, R. Lage, P. B. Martínez de Morentin, S. Tovar, R. Nogueiras, D. Carling, C. Lelliott, R. Gallego, M. Oresic, K. Chatterjee, A. K. Saha, K. Rahmouni, C. Diéguez, A. Vidal-Puig, Hypothalamic AMPK and fatty acid metabolism mediate thyroid regulation of energy balance. *Nat. Med.* **16**, 1001–1008 (2010).
7. T. Shiuchi, M. S. Haque, S. Okamoto, T. Inoue, H. Kageyama, S. Lee, C. Toda, A. Suzuki, E. S. Bachman, Y.-B. B. Kim, T. Sakurai, M. Yanagisawa, S. Shioda, K. Imoto, Y. Minokoshi, Hypothalamic orexin stimulates feeding-associated glucose utilization in skeletal muscle via sympathetic nervous system. *Cell Metab.* **10**, 466–480 (2009).
8. C. K. Gavini, W. C. Jones, C. M. Novak, Ventromedial hypothalamic melanocortin receptor activation: Regulation of activity energy expenditure and skeletal muscle thermogenesis. *J. Physiol.* **594**, 5285–5301 (2016).
9. Y. Minokoshi, Y.-B. Kim, O. D. Peroni, L. G. D. Fryer, C. Müller, D. Carling, B. B. Kahn, Leptin stimulates fatty-acid oxidation by activating AMP-activated protein kinase. *Nature* **415**, 339–343 (2002).
10. K. Timper, J. L. Denson, S. M. Steculorum, C. Heilinger, L. Engström-Ruud, C. M. Wunderlich, S. Rose-John, F. T. Wunderlich, J. C. Brüning, IL-6 Improves energy and glucose homeostasis in obesity via enhanced central IL-6 trans-signaling. *Cell Rep.* **19**, 267–280 (2017).
11. V. C. Bobbo, D. F. Engel, C. P. Jara, N. F. Mendes, R. Haddad-Tovolli, T. P. Prado, D. Sidarta-Oliveira, J. Morari, L. A. Velloso, E. P. Araujo, Interleukin-6 actions in the hypothalamus protects against obesity and is involved in the regulation of neurogenesis. *J. Neuroinflammation* **18**, 192 (2021).
12. D. Mishra, J. E. Richard, I. Maric, B. Porteiro, M. Häring, S. Kooijman, S. Musovic, K. Eerola, L. López-Ferreras, E. Peris, K. Grycel, O. T. Shevchouk, P. Micallef, C. S. Olofsson, I. Wernstedt Asterholm, H. J. Grill, R. Nogueiras, K. P. Skibicka, Parabrachial interleukin-6 reduces body weight and food intake and increases thermogenesis to regulate energy metabolism. *Cell Rep.* **26**, 3011–3026.e5 (2019).
13. V. Wallenius, K. Wallenius, B. Ahrén, M. Rudling, H. Carlsten, S. L. Dickson, C. Ohlsson, J.-O. Jansson, Interleukin-6-deficient mice develop mature-onset obesity. *Nat. Med.* **8**, 75–79 (2002).
14. E. R. Ropelle, M. B. Flores, D. E. Cintra, G. Z. Rocha, J. R. Pauli, J. Morari, C. T. de Souza, J. C. Moraes, P. O. Prada, D. Guadagnini, R. M. Marin, A. G. Oliveira, T. M. Augusto, H. F. Carvalho, L. A. Velloso, M. J. A. Saad, J. B. C. Carvalheira, IL-6 and IL-10 anti-inflammatory activity links exercise to hypothalamic insulin and leptin sensitivity through IKKβ and ER stress inhibition. *PLOS Biol.* **8**, e1000465 (2010).
15. J. Lonsdale, J. Thomas, M. Salvatore, R. Phillips, E. Lo, S. Shad, R. Hasz, G. Walters, F. Garcia, N. Young, B. Foster, M. Moser, E. Karasik, B. Gillard, K. Ramsey, S. Sullivan, J. Bridge, H. Magazine, J. Syron, J. Fleming, L. Siminoff, H. Traino, M. Mosavel, L. Barker, S. Jewell, D. Rohrer, D. Maxim, D. Filkins, P. Harbach, E. Cortadillo, B. Berghuis, L. Turner, E. Hudson, K. Feenstra, L. Sobin, J. Robb, P. Branton, G. Korzeniewski, C. Shive, D. Tabor, L. Qi, K. Groch, S. Nampally, S. Buia, A. Zimmerman, A. Smith, R. Burges, K. Robinson, K. Valentino, D. Bradbury, M. Cosentino, N. Diaz-Mayoral, M. Kennedy, T. Engel, P. Williams, K. Erickson, K. Ardlie, W. Winckler, G. Getz, D. DeLuca, D. MacArthur, M. Kellis, A. Thomson, T. Young, E. Gelfand, M. Donovan, Y. Meng, G. Grant, D. Mash, Y. Marcus, M. Basile, J. Liu, J. Zhu, Z. Tu, N. J. Cox, D. L. Nicolae, E. R. Gamazon, H. K. Im, A. Konkashbaev, J. Pritchard, M. Stevens, T. Flutre, X. Wen, E. T. Dermitzakis, T. Lappalainen, R. Guigo, J. Monlong, M. Sammeth, D. Koller, A. Battle, S. Mostafavi, M. McCarthy, M. Rivas, J. Maller, I. Rusyn, A. Nobel, F. Wright, A. Shabalin, M. Feolo, N. Sharopova, A. Sturcke, J. Paschal, J. M. Anderson, E. L. Wilder, L. K. Derr, E. D. Green, J. P. Struewing, G. Temple, S. Volpi, J. T. Boyer, E. J. Thomson, M. S. Guyer, C. Ng, A. Abdallah, D. Colantuoni, T. R. Insel, S. E. Koester, A. R. Little, P. K. Bender, T. Lehner, Y. Yao, C. C. Compton, J. B. Vaught, S. Sawyer, N. C. Lockhart, J. Demchok, H. F. Moore, The Genotype-Tissue Expression (GTEx) project. *Nat. Genet.* **45**, 580–585 (2013).
16. P. A. Andreux, E. G. Williams, H. Koutnikova, R. H. Houtkooper, M.-F. Champy, H. Henry, K. Schoonjans, R. W. Williams, J. Auwerx, Systems genetics of metabolism: The use of the BXD murine reference panel for multiscalar integration of traits. *Cell* **150**, 1287–1299 (2012).
17. H. Schwarz, M. Schmittner, A. Duschl, J. Horejs-Hoeck, Residual Endotoxin contaminations in recombinant proteins are sufficient to activate human CD1c+ dendritic cells. *PLOS ONE* **9**, e113840 (2014).
18. A. Poltorak, X. He, I. Smirnova, M. Y. Liu, C. van Huffel, X. Du, D. Birdwell, E. Alejos, M. Silva, C. Galanos, M. Freudenberg, P. Ricciardi-Castagnoli, B. Layton, B. Beutler, Defective LPS signaling in C3H/HeJ and C57BL/10ScCr mice: Mutations in Tlr4 gene. *Science* **282**, 2085–2088 (1998).
19. S. T. Qureshi, L. Larivière, G. Leveque, S. Clermont, K. J. Moore, P. Gros, D. Malo, Endotoxin-tolerant mice have mutations in toll-like receptor 4 (Tlr4). *J. Exp. Med.* **189**, 615–625 (1999).
20. C. Toda, T. Shiuchi, H. Kageyama, S. Okamoto, E. A. Coutinho, T. Sato, Y. Okamatsu-Ogura, S. Yokota, K. Takagi, L. Tang, K. Saito, S. Shioda, Y. Minokoshi, T. Tang, K. Saito, S. Shioda, Y. Minokoshi, Extracellular signal-regulated kinase in the ventromedial hypothalamus mediates leptin-induced glucose uptake in red-type skeletal muscle. *Diabetes* **62**, 2295–2307 (2013).
21. S.-J. Kim, N. Guerrero, G. Wassef, J. Xiao, H. H. Mehta, P. Cohen, K. Yen, The mitochondrial-derived peptide humanin activates the ERK1/2, AKT, and STAT3 signaling pathways and has age-dependent signaling differences in the hippocampus. *Oncotarget* **7**, 46899–46912 (2016).
22. X.-X. Fang, X.-L. Jiang, X.-H. Han, Y.-P. Peng, Y.-H. Qiu, Neuroprotection of interleukin-6 against NMDA-induced neurotoxicity is mediated by JAK/STAT3, MAPK/ERK, and PI3K/AKT signaling pathways. *Cell. Mol. Neurobiol.* **33**, 241–251 (2013).
23. K. Rahmouni, C. D. Sigmund, W. G. Haynes, A. L. Mark, Hypothalamic ERK mediates the anorectic and thermogenic sympathetic effects of leptin. *Diabetes* **58**, 536–542 (2009).
24. M. Tanida, H. Gotoh, N. Yamamoto, M. Wang, Y. Kuda, Y. Kurata, M. Mori, T. Shibamoto, Hypothalamic nesfatin-1 stimulates sympathetic nerve activity via hypothalamic ERK signaling. *Diabetes* **64**, 3725–3736 (2015).
25. S. H. Cha, Z. Hu, S. Chohnan, M. D. Lane, Inhibition of hypothalamic fatty acid synthase triggers rapid activation of fatty acid oxidation in skeletal muscle. *Proc. Natl. Acad. Sci. U.S.A.* **102**, 14557–14562 (2005).
26. N. E. Kimber, D. Cameron-Smith, S. L. McGee, M. Hargreaves, Skeletal muscle fat metabolism after exercise in humans: Influence of fat availability. *J. Appl. Physiol.* **114**, 1577–1585 (2013).
27. G. C. Henderson, B. L. Alderman, Determinants of resting lipid oxidation in response to a prior bout of endurance exercise. *J. Appl. Physiol.* **116**, 95–103 (2014).
28. D. Malatesta, C. Werlen, S. Bulfaro, X. Chenevière, F. Borrani, Effect of high-intensity interval exercise on lipid oxidation during postexercise recovery. *Med. Sci. Sports Exerc.* **41**, 364–374 (2009).
29. N. Nadermann, H. Volkoff, Effects of short-term exercise on food intake and the expression of appetite-regulating factors in goldfish. *Peptides* **123**, 170182 (2020).
30. L. Nybo, B. Nielsen, B. K. Pedersen, K. Møller, N. H. Secher, Interleukin-6 release from the human brain during prolonged exercise. *J. Physiol.* **542**, 991–995 (2002).
31. S. L. Bowers, S. D. Bilbo, F. S. Dhabhar, R. J. Nelson, Stressor-specific alterations in corticosterone and immune responses in mice. *Brain Behav. Immun.* **22**, 105–113 (2008).
32. G. van Hall, A. Steensberg, M. Sacchetti, C. Fischer, C. Keller, P. Schjerling, N. Hiscock, K. Møller, B. Saltin, M. A. Febbraio, B. K. Pedersen, Interleukin-6 stimulates lipolysis and fat oxidation in humans. *J. Clin. Endocrinol. Metab.* **88**, 3005–3010 (2003).
33. B. Lukaszuk, I. Bialuk, J. Górski, M. Zajączkiewicz, M. M. Winnicka, A. Chabowski, A single bout of exercise increases the expression of glucose but not fatty acid transporters in skeletal muscle of IL-6 KO mice. *Lipids* **47**, 763–772 (2012).
34. A. L. Carey, G. R. Steinberg, S. L. Macaulay, W. G. Thomas, A. G. Holmes, G. Ramm, O. Prelovsek, C. Hohnen-Behrens, M. J. Watt, D. E. James, B. E. Kemp, B. K. Pedersen, M. A. Febbraio, Interleukin-6 increases insulin-stimulated glucose disposal in humans and glucose uptake and fatty acid oxidation in vitro via AMP-activated protein kinase. *Diabetes* **55**, 2688–2697 (2006).
35. L. M. Harden, I. du Plessis, S. Poole, H. P. Laburn, Interleukin (IL)-6 and IL-1 beta act synergistically within the brain to induce sickness behavior and fever in rats. *Brain Behav. Immun.* **22**, 838–849 (2008).
36. J. Fäldt, I. Wernstedt, S. M. Fitzgerald, K. Wallenius, G. Bergström, J.-O. Jansson, Reduced exercise endurance in interleukin-6-deficient mice. *Endocrinology* **145**, 2680–2686 (2004).
37. E. Schéle, A. Benrick, L. Grahnemo, E. Egecioglu, F. Anesten, V. Pálsdóttir, J.-O. Jansson, Inter-relation between interleukin (IL)-1, IL-6 and body fat regulating circuits of the hypothalamic arcuate nucleus. *J. Neuroendocrinol.* **25**, 580–589 (2013).
38. R. Jankord, R. Zhang, J. N. Flak, M. B. Solomon, J. Albertz, J. P. Herman, Stress activation of IL-6 neurons in the hypothalamus. *Am. J. Physiol. Regul. Integr. Comp. Physiol.* **299**, R343–R351 (2010).
39. M. A. Febbraio, Gp130 receptor ligands as potential therapeutic targets for obesity. *J. Clin. Invest.* **117**, 841–849 (2007).
40. Y. Song, J. Altarejos, M. O. Goodarzi, H. Inoue, X. Guo, R. Berdeaux, J.-H. Kim, J. Goode, M. Igata, J. C. Paz, M. F. Hogan, P. K. Singh, N. Goebel, L. Vera, N. Miller, J. Cui, M. R. Jones, Y.-D. I. Chen, K. D. Taylor, W. A. Hsueh, J. I. Rotter, M. Montminy, CRTC3 links catecholamine signalling to energy balance. *Nature* **468**, 933–939 (2010).
41. H. Tsuneki, E. Tokai, Y. Nakamura, K. Takahashi, M. Fujita, T. Asaoka, K. Kon, Y. Anzawa, T. Wada, I. Takasaki, K. Kimura, H. Inoue, M. Yanagisawa, T. Sakurai, T. Sasaoka,

Hypothalamic orexin prevents hepatic insulin resistance via daily bidirectional regulation of autonomic nervous system in mice. *Diabetes* **64**, 459–470 (2015).
42. X. Liu, Y. Niu, H. Yuan, J. Huang, L. Fu, AMPK binds to Sestrins and mediates the effect of exercise to increase insulin-sensitivity through autophagy. *Metab. Clin. Exp.* **64**, 658–665 (2015).
43. C. He, M. C. Bassik, V. Moresi, K. Sun, Y. Wei, Z. Zou, Z. An, J. Loh, J. Fisher, Q. Sun, S. Korsmeyer, M. Packer, H. I. May, J. A. Hill, H. W. Virgin, C. Gilpin, G. Xiao, R. Bassel-Duby, P. E. Scherer, B. Levine, Exercise-induced BCL2-regulated autophagy is required for muscle glucose homeostasis. *Nature* **481**, 511–515 (2012).
44. J. R. Pauli, E. R. Ropelle, D. E. Cintra, M. A. Carvalho-Filho, J. C. Moraes, C. T. De Souza, L. A. Velloso, J. B. C. Carvalheira, M. J. A. Saad, Acute physical exercise reverses S-nitrosation of the insulin receptor, insulin receptor substrate 1 and protein kinase B/Akt in diet-induced obese Wistar rats. *J. Physiol.* **586**, 659–671 (2008).
45. R. Kjøbsted, A. J. T. Pedersen, J. R. Hingst, R. Sabaratnam, J. B. Birk, J. M. Kristensen, K. Højlund, J. F. P. Wojtaszewski, Intact regulation of the AMPK signaling network in response to exercise and insulin in skeletal muscle of male patients with type 2 diabetes: Illumination of AMPK activation in recovery from exercise. *Diabetes* **65**, 1219–1230 (2016).
46. J. Norrbom, E. K. Sällstedt, H. Fischer, C. J. Sundberg, H. Rundqvist, T. Gustafsson, Alternative splice variant PGC-1α-b is strongly induced by exercise in human skeletal muscle. *Am. J. Physiol. Endocrinol. Metab.* **301**, E1092–E1098 (2011).
47. R. S. Lee-Young, M. J. Palmer, K. C. Linden, K. LePlastrier, B. J. Canny, M. Hargreaves, G. D. Wadley, B. E. Kemp, G. K. McConell, Carbohydrate ingestion does not alter skeletal muscle AMPK signaling during exercise in humans. *Am. J. Physiol. Endocrinol. Metab.* **291**, E566–E573 (2006).
48. R. R. Mason, R. C. R. Meex, R. Lee-Young, B. J. Canny, M. J. Watt, Phosphorylation of adipose triglyceride lipase Ser(404) is not related to 5′-AMPK activation during moderate-intensity exercise in humans. *Am. J. Physiol. Endocrinol. Metab.* **303**, E534–E541 (2012).
49. B. Trinh, M. Peletier, C. Simonsen, P. Plomgaard, K. Karstoft, B. K. Pedersen, G. Van Hall, H. Ellingsgaard, Blocking endogenous IL-6 impairs mobilization of free fatty acids during rest and exercise in lean and obese men. *Cell Rep. Med.* **2**, 100396 (2021).
50. A.-S. Wedell-Neergaard, L. Lang Lehrskov, R. H. Christensen, G. E. Legaard, E. Dorph, M. K. Larsen, N. Launbo, S. R. Fagerlind, S. K. Seide, S. Nymand, M. Ball, N. Vinum, C. N. Dahl, M. Henneberg, M. Ried-Larsen, J. D. Nybing, R. Christensen, J. B. Rosenmeier, K. Karstoft, B. K. Pedersen, H. Ellingsgaard, R. Krogh-Madsen, Exercise-induced changes in visceral adipose tissue mass are regulated by IL-6 signaling: A randomized controlled trial. *Cell Metab.* **29**, 844–855.e3 (2019).
51. Q. Wu, Y. Chen, W. Zhang, S. Song, Z. Xu, H. Zhang, L. Liu, J. Sun, Upregulation of chemokines in the paraventricular nucleus of the hypothalamus in rats with stress-induced hypertension. *Med. Sci. Monit.* **26**, e926807 (2020).
52. V. C. D. Bobbo, C. P. Jara, N. F. Mendes, J. Morari, L. A. Velloso, E. P. Araújo, Interleukin-6 expression by hypothalamic microglia in multiple inflammatory contexts: A systematic review. *Biomed. Res. Int.* **2019**, 1365210 (2019).
53. L. Hein, J. D. Altman, B. K. Kobilka, Two functionally distinct α_2-adrenergic receptors regulate sympathetic neurotransmission. *Nature* **402**, 181–184 (1999).
54. V. R. Muñoz, R. C. Gaspar, M. B. Severino, A. P. A. Macêdo, F. M. Simabuco, E. R. Ropelle, D. E. Cintra, A. S. R. da Silva, Y.-B. Kim, J. R. Pauli, Exercise counterbalances Rho/ROCK2 signaling impairment in the skeletal muscle and ameliorates insulin sensitivity in obese mice. *Front. Immunol.* **12**, 702025 (2021).
55. J. Chen, K. Fujii, L. Zhang, T. Roberts, H. Fu, Raf-1 promotes cell survival by antagonizing apoptosis signal-regulating kinase 1 through a MEK-ERK independent mechanism. *Proc. Natl. Acad. Sci. U.S.A.* **98**, 7783–7788 (2001).
56. J. J. Brady, M. Li, S. Suthram, H. Jiang, W. H. Wong, H. M. Blau, Early role for IL-6 signalling during generation of induced pluripotent stem cells revealed by heterokaryon RNA-Seq. *Nat. Cell Biol.* **15**, 1244–1252 (2013).
57. M. Crettaz, M. Prentki, D. Zaninetti, B. Jeanrenaud, Insulin resistance in soleus muscle from obese Zucker rats. Involvement of several defective sites. *Biochem. J.* **186**, 525–534 (1980).
58. B. Leighton, L. Budohoski, F. J. Lozeman, R. A. Challiss, E. A. Newsholme, The effect of prostaglandins E1, E2 and F2 alpha and indomethacin on the sensitivity of glycolysis and glycogen synthesis to insulin in stripped soleus muscles of the rat. *Biochem. J.* **227**, 337–340 (1985).
59. N. Shirai, H. Suzuki, S. Wada, Direct methylation from mouse plasma and from liver and brain homogenates. *Anal. Biochem.* **343**, 48–53 (2005).
60. B. Xue, T. Pulinilkunnil, I. Murano, K. K. Bence, H. He, Y. Minokoshi, K. Asakura, A. Lee, F. Haj, N. Furukawa, K. J. Catalano, M. Delibegovic, J. A. Balschi, S. Cinti, B. G. Neel, B. B. Kahn, Neuronal protein tyrosine phosphatase 1B deficiency results in inhibition of hypothalamic AMPK and isoform-specific activation of AMPK in peripheral tissues. *Mol. Cell. Biol.* **29**, 4563–4573 (2009).
61. F. Chiappini, K. J. Catalano, J. Lee, O. D. Peroni, J. Lynch, A. S. Dhaneshwar, K. Wellenstein, A. Sontheimer, B. G. Neel, B. B. Kahn, Ventromedial hypothalamus-specific Ptpn1 deletion exacerbates diet-induced obesity in female mice. *J. Clin. Invest.* **124**, 3781–3792 (2014).
62. C. C. Parker, P. E. Dickson, V. M. Philip, M. Thomas, E. J. Chesler, Systems genetic analysis in GeneNetwork.org. *Curr. Protoc. Neurosci.* **79**, 8.39.1–8.39.20 (2017).
63. R. A. Irizarry, B. Hobbs, F. Collin, Y. D. Beazer-Barclay, K. J. Antonellis, U. Scherf, T. P. Speed, Exploration, normalization, and summaries of high density oligonucleotide array probe level data. *Biostatistics* **4**, 249–264 (2003).

Acknowledgments: We thank J. Auwerx from EPFL, Switzerland for assistance with the bioinformatics analysis; N. Robson de Almeida from the University of São Paulo (USP) for maintaining the α2AC KO mice; G. Rocha, L. Lenhare, K. Rodrigues, and J. Camargo for technical assistance; and M. A. Kurauti for providing the IL6 ELISA kit. We acknowledge the technical support of M. O. Baratti and the National Institute of Science and Technology of Photonics Applied to Cell Biology (INFABIC) for aid with confocal microscopy. **Funding:** This work was supported by grants from the São Paulo Research Foundation–FAPESP scholarships (2012/23006-1, 2013/26053-3, and 2018/04192-5), research projects (2019/21709-4 and 2019-11820-5), Brazilian National Council for Scientific and Technological Development–CNPq (477478/2012-3), and Coordination for the Improvement of Higher Education Personnel (CAPES) number 001. L.J.E.G. was supported by the European Union's Horizon 2020 research and innovation programme through the Marie Skłodowska-Curie Individual Fellowship "AmyloAge" (grant agreement no. 896042). **Author contributions:** C.K.K. and T.d.O.M. performed Western blot analysis. C.K.K., T.d.O.M., and V.R.R.S. performed oxygen consumption and PCR analysis in IL6-injected mice. R.R.B. performed immunofluorescence experiments. A.M.-A. performed lentivirus assays. R.S.B. performed PCR analysis in the time-course study of exercised mice. M.R.T. and F.M.S. performed N2A cell experiments. C.K.K. performed denervation experiments. C.K.K. and B.M.C. performed stereotaxic surgeries and blue dye staining. C.d.O.R. and D.E.C. performed mass spectrometry analysis. R.S.G. and E.R.R. performed bioinformatics analysis. T.d.O.M., P.P., D.G.-T., M.d.C.G., A.L.d.R., and S.T. contributed to all IL6KO experiments. T.d.O.M., S.M.H., and J.C.R.N. performed fatty acid oxidation assays. R.S.G. performed RNA sequencing analysis. L.J.E.G. performed bioinformatics analysis in fig. S2. P.C.B. provided α2AC KO mice. P.O.P. and R.R.B. conducted the VMH dissection experiment. V.A.M. and L.B. prepared the confocal assay. H.M.-S. supervised confocal microscopy experiments. R.C., A.S.R.d.S., L.P.d.M., J.R.P., D.E.C., and L.A.V. provided laboratory support and contributed to the discussion. E.R.R. wrote the manuscript. **Competing interests:** The authors declare that they have no competing interests. **Data and materials availability:** All data needed to evaluate the conclusions in the paper are present in the paper and/or the Supplementary Materials.

Submitted 7 October 2021
Accepted 15 June 2022
Published 29 July 2022
10.1126/sciadv.abm7355

ScienceAdvances

Evidence for a neuromuscular circuit involving hypothalamic interleukin-6 in the control of skeletal muscle metabolism

Carlos Kiyoshi KatashimaThayana de Oliveira MichelettiRenata Rosseto BragaRodrigo Stellzer GasparLudger J. E. GoeminneAlexandre Moura-AssisBarbara Moreira CrisolRafael S. BrícolaVagner Ramon R. SilvaCamila de Oliveira RamosAlisson L. da RochaMariana Rosolen TavaresFernando Moreira SimabucoValquiria Aparecida MatheusLucas BuscarattiHenrique Marques-SouzaPatricia PazosDavid Gonzalez-ToucedaSulay TovarMaría del Carmen GarcíaJose Cesar Rosa NetoRui CuriSandro Massao HirabaraPatrícia Chakur BrumPatrícia Oliveira PradaLeandro P. de MouraJosé Rodrigo PauliAdelino S. R. da SilvaDennys Esper CintraLicio A. VellosoEduardo Rochete Ropelle

Sci. Adv., 8 (30), eabm7355. • DOI: 10.1126/sciadv.abm7355

Science Advances (ISSN) is published by the American Association for the Advancement of Science. 1200 New York Avenue NW, Washington, DC 20005. The title *Science Advances* is a registered trademark of AAAS.